PHOTOGRAPH THIS SHEET

DTIC ACCESSION NUMBER

LEVEL

INVENTORY

DOCUMENT IDENTIFICATION

HANDLE WITH CARE

DISTRIBUTION STATEMENT

ACCESSION FOR

NTIS GRA&I ☐

DTIC TRAC ☐

UNANNOUNCED ☐

JUSTIFICATION

BY

DISTRIBUTION/

AVAILABILITY CODES

DISTRIBUTION	AVAILABILITY AND/OR SPECIAL	

DISTRIBUTION STAMP

DATE ACCESSIONED

DATE RETURNED

DATE RECEIVED IN DTIC

REGISTERED OR CERTIFIED NUMBER

PHOTOGRAPH THIS SHEET AND RETURN TO DTIC-FDAC

DTIC FORM 70A JUN 90

DOCUMENT PROCESSING SHEET

PREVIOUS EDITIONS MAY BE USED UNTIL STOCK IS EXHAUSTED.

ESD-TR-79-319
ESL-TR-80-09

Final Report

Remote Sensing of Turbine Engine Gases

30 September 1979

Prepared for the Department of the Air Force
under Electronic Systems Division Contract F19628-78-C-0002 by

Lincoln Laboratory

MASSACHUSETTS INSTITUTE OF TECHNOLOGY

LEXINGTON, MASSACHUSETTS

The work reported in this document was performed at Lincoln Laboratory, a center for research operated by Massachusetts Institute of Technology. This work was supported by the Department of the Air Force under Contract F19628-78-C-0002, in part with specific funding from the Engineering and Services Laboratory, Air Force Engineering and Services Center, Tyndall Air Force Base, Florida.

This technical report has been reviewed and is approved for publication.

FOR THE COMMANDER

Raymond L. Loiselle

Raymond L. Loiselle, Lt. Col., USAF
Chief, ESD Lincoln Laboratory Project Office

MASSACHUSETTS INSTITUTE OF TECHNOLOGY
LINCOLN LABORATORY

REMOTE SENSING OF TURBINE ENGINE GASES

A. MOORADIAN
D. K. KILLINGER
N. MENYUK
Group 82

FINAL REPORT
TO THE
AIR FORCE ENGINEERING AND SERVICES CENTER

15 JULY 1978 – 30 SEPTEMBER 1979

ISSUED 18 MARCH 1980

LEXINGTON MASSACHUSETTS

Table of Contents

		page
I.	Introduction	1
II.	Development of Improved Repetition Rate Miniature CO_2 TEA Laser System	1
III.	Laboratory Demonstration of CO_2 Laser System	2
IV.	Initial Field Feasibility Demonstration	3
V.	Conclusions and Recommendations	5
	Appendix A: Development of a High Repetition Rate Mini-TEA CO_2 Laser	10
	Appendix B: Preferred Frequencies for Remote Sensing of CO and NO	29
	Appendix C: Possible Frequencies for the Remote Sensing of C_2H_4, NH_3, O_3, and CH_3OH	41
	Appendix D: Range and Sensitivity Considerations of a Frequency-Doubled Mini-TEA CO_2 Laser for Remote Sensing of CO and NO	50
	Appendix E: Remote Sensing of CO Using Frequency-Doubled CO_2 Laser Radiation	67

I. INTRODUCTION

This document is the final report for a laser remote sensing research program conducted by Lincoln Laboratory with support by the Department of the Air Force, in part with specific funding from the Air Force Engineering and Services Center. The research conducted was designed to develop and demonstrate laser remote sensing techniques for monitoring jet aircraft exhaust gases. This effort was part of a larger Lincoln Laboratory program to develop remote sensing techniques for environmental monitoring and tactical detection and discrimination. The effort was carried out at the Lincoln Laboratory Laser Remote Sensing Facility, and was able to take advantage of its location directly adjacent to Hanscom AFB. A photograph of the Laser Remote Sensing Facility and surrounding area is shown in Fig. 1.

The specific tasks which were performed for this research program consisted of the following: (1) development of an improved repetition rate miniature CO_2 TEA laser and incorporation into a differential-absorption LIDAR (DIAL) system, (2) laboratory demonstration of the frequency-doubled CO_2 TEA laser system by differential-absorption measurements of known gas samples (CO and NO), and (3) initial field feasibility demonstration of laser remote detection of CO in vehicular exhaust (automobile, tractor mower and Skycrane helicopter) at ranges up to 2.5 km.

Each of these tasks is described in detail in the following sections of this report. In addition, supportive documentation is included in the accompanying appendices.

II. DEVELOPMENT OF IMPROVED REPETITION RATE MINIATURE CO_2 TEA LASER SYSTEM

A stable, line-tunable, frequency-doubled mini-TEA CO_2 laser system was developed which was utilized in subsequent remote sensing measurements of atmospheric CO. Details of the mini-TEA CO_2 laser are presented in Appendix A, which is a preprint of an article to appear in the Review of Scientific Instruments. The mini-TEA laser described is of a relatively simple, compact design with a 1.8 cm^3 active volume. The laser is capable of operating at 500 Hz and with pulse energies on the order of 40 mJ/pulse.

The device is line tunable over approximately 50 CO_2 laser transitions and has a nearly diffraction-limited output. This mini-TEA laser has been operated on a semi-continuous basis for over 50 million shots without any significant reduction in system performance.

The output from the mini-TEA laser was frequency-doubled by use of a $CdGeAs_2$ crystal grown at Lincoln Laboratory. Output power at 5 μm was approximately 0.2-2 mJ/pulse.

The frequency-doubled laser source was then integrated into a remote sensing DIAL system including transmission and reception optics, a detector, and associated electronics. The system was set up in the Laboratory's Laser Remote Sensing Facility.

III. LABORATORY DEMONSTRATION OF CO_2 TEA LASER SYSTEM

A laboratory demonstration of the frequency-doubled CO_2 TEA laser system was conducted by making differential-absorption measurements of known gas samples in optical cells. These measurements were compared to predicted theoretical differential-absorption calculations. The specific theoretical predictions are contained in Lincoln Laboratory memos and are presented in Appendices B and C. A synopsis of each appendix, associated conclusions, and comparison with experimental results where appropriate are given below.

Appendix B ("Preferred Frequencies for Remote Sensing of CO and NO") presents the rationale for the selection of particular frequency-doubled laser transitions for the laser remote sensing of CO and NO in the atmosphere. As detailed in Appendix B, CO in the atmosphere may be detected using either the doubled R(18) laser transition of CO_2 near 2154.604 cm^{-1} with the R(2) absorption line of CO near 2154.596 cm^{-1}, or the doubled P(24) laser transition of CO_2 near 2086.326 cm^{-1} with the P(14) absorption line of CO near 2086.322 cm^{-1}. On the other hand, the detection of NO in the atmosphere is hindered by the strong interference due to water vapor; only the doubled P(24) CO_2 laser transition near 1973 cm^{-1} has a coincidence with an NO absorption line which lies in an atmospheric transmission window relatively free from interference due to water vapor.

Laboratory experiments were conducted to verify the above theoretical predictions. These experiments indicated that the measured absolute and differential-absorption coefficients for CO and NO were in agreement within our experimental uncertainty (± 10%) with the theoretical predictions. However, significant discrepancies in the differential-absorption coefficients of the interference background due to water vapor at frequencies near the NO absorption transitions were measured.

Appendix C ("Possible Frequencies for the Remote Sensing of C_2H_4, NH_3, O_3, and CH_3OH") presents coincidences of both the fundamental and the frequency-doubled CO_2 laser transition with the various molecular absorption lines. While the data presented in Appendix C is not directly used in the experimental research detailed in this report, it is presented since it serves as a reference for future experimental research.

IV. INITIAL FIELD FEASIBILITY MEASUREMENTS

4.1 Preliminary Studies

Preliminary theoretical studies were conducted to predict the detection range for a differential-absorption, frequency-doubled CO_2 LIDAR system. In particular, calculations were made for the laser remote sensing of CO, NO, and C_2H_4, as well as other molecules (ammonia, ozone, and methanol) in the atmosphere using differential-absorption of frequency-doubled CO_2 laser radiation backscattered from topographic targets. These studies are presented in Appendix D which is a reprint of a Lincoln Laboratory memo. A synopsis of this appendix is given below.

Appendix D ("Range and Sensitivity Considerations of a Frequency-Doubled Mini-TEA CO_2 Laser for Remote Sensing of CO and NO") utilizes the information presented in Appendices B and C and calculates the predicted DIAL detection range for a localized pocket of gaseous effluent. The calculations indicate that a 5-μm DIAL system operating with approximately 1 mJ/pulse should be capable of detecting a localized pocket of CO, NO, or C_2H_4 (100 ppm contained within a distance of 50 m) at ranges of 1-3 km.

Utilizing the high PRF (500 Hz) capability of the mini-TEA CO_2 laser, it is expected that the signal average of up to 1,000 pulses (2 seconds of data) may be obtained. Under such conditions, the expected detection ranges for C_2H_4, NO, and CO under midlatitude summer (high humidity) conditions is approximately 10, 2, and 8 km, respectively. Detection ranges under winter (low humidity) conditions are higher.

As seen from the above synopsis of the theoretical analysis presented in Appendix D, a high PRF, moderate power 5-μm DIAL system should be capable of the laser remote sensing of CO, NO, and C_2H_4 at moderate ranges (1-10 km). The experimental verification of the predictions for CO, is presented in the following sections of this report.

4.2 Measurements of Atmospheric CO

The DIAL system described in Section II was used to make single-ended remote sensing measurements of the atmospheric concentration of CO. The concentration of CO was deduced from laser backscatter returns from topographic targets at ranges up to 2.5 km with an overall uncertainty of approximately ± 10 ppb. Details of the experimental apparatus, experimental procedure and measurement results are presented in Appendix E, which is a preprint of a journal article to appear in Applied Physics Letters.

As described in Appendix E, the following major experimental laser remote sensing measurements were conducted:

1) Detection of average day-to-day atmospheric CO concentration on the order of 150-250 ppb (parts per billion). These measurements were obtained at ranges up to 2.5 km using targets such as the flight facility (hangar) shown in Fig. 1. Uncertainties in the measurements were on the order of ± 10 ppb; the effect of atmospheric turbulence contributed an uncertainty on the order of ± 2 ppb/km.
2) The diurnal variation of CO concentration located over a major traffic roadway was measured. Concentrations as high

as 2,000 ppb were observed during periods of heavy traffic. The increase in CO concentration due to individual vehicles as they passed the laser path was measured.

3) The pseudo-range-resolved concentration of CO was deduced by differentiating the integrated measurements obtained from backscatter from various targets located at different ranges, but along the same line-of-sight. These measurements clearly established the strong localization of CO over the traffic roadway.

4.3 Preliminary Detection of CO in the Exhaust of a Skycrane Helicopter

During the long-range (2.5 km) laser remote sensing measurements of CO described above, various exhaust emitting targets approached the transmitted laser beam. Short-term increases in the measured CO concentration on the order of 50-100 ppb were observed to be correlated with aircraft or vehicular (tractor mower) movement near the laser line-of-sight. An example of such data is shown in Fig. 2. These measurements indicate the increase in the CO concentration when a turbine-powered Skycrane helicopter landed within 50 m of the laser line-of-sight at a range of 2.4 km; the measured localized CO concentration near the aircraft was greater than 2 ppm if it is assumed that the increased CO concentration over the ambient level was confined to a region within 50 m of the aircraft.

The preliminary measurements presented above, which were obtained with targets of opportunity, clearly indicate that the present differential-absorption system is capable of the single-ended remote sensing of engine exhaust gases.

V. CONCLUSIONS AND RECOMMENDATIONS

The research program detailed in this report has demonstrated the feasibility of the laser remote sensing of atmospheric CO at ranges of up to 2.5 km. In addition, initial experiments have indicated the remote

detection of localized pockets of CO produced by the exhaust from a wide range of vehicles, such as cars, trucks, farm tractors, and helicopters.

It is recommended that further research be conducted in the following areas:

1) Quantitative DIAL measurements of exhaust pollutants using vehicles with known effluent production.

2) Expansion of DIAL measurements to include the remote sensing of NO and C_2H_4.

3) Introduction of a high-speed digital data acquisition system fast enough to handle the high-repetition capability of the present mini-TEA laser. It is anticipated that such a system will increase the available signal-to-noise ratio by one to two orders of magnitude.

FIGURE CAPTIONS

Figure 1. Photograph of Lincoln Laboratory Laser Remote Sensing Facility (white building on roof at left of photo) and adjacent Hanscom Air Force Base. The facility provides a dedicated laboratory for the testing of laser remote sensing techniques and commands an unobstructed view of various topographic targets including cars, aircraft hangars, fuel storage tanks; mountains as far away as 30 miles are observable from this location.

Figure 2. Laser remote sensing of atmospheric CO concentration indicating detection of vehicular exhaust at a range of 2.5 km.

Fig. 1.

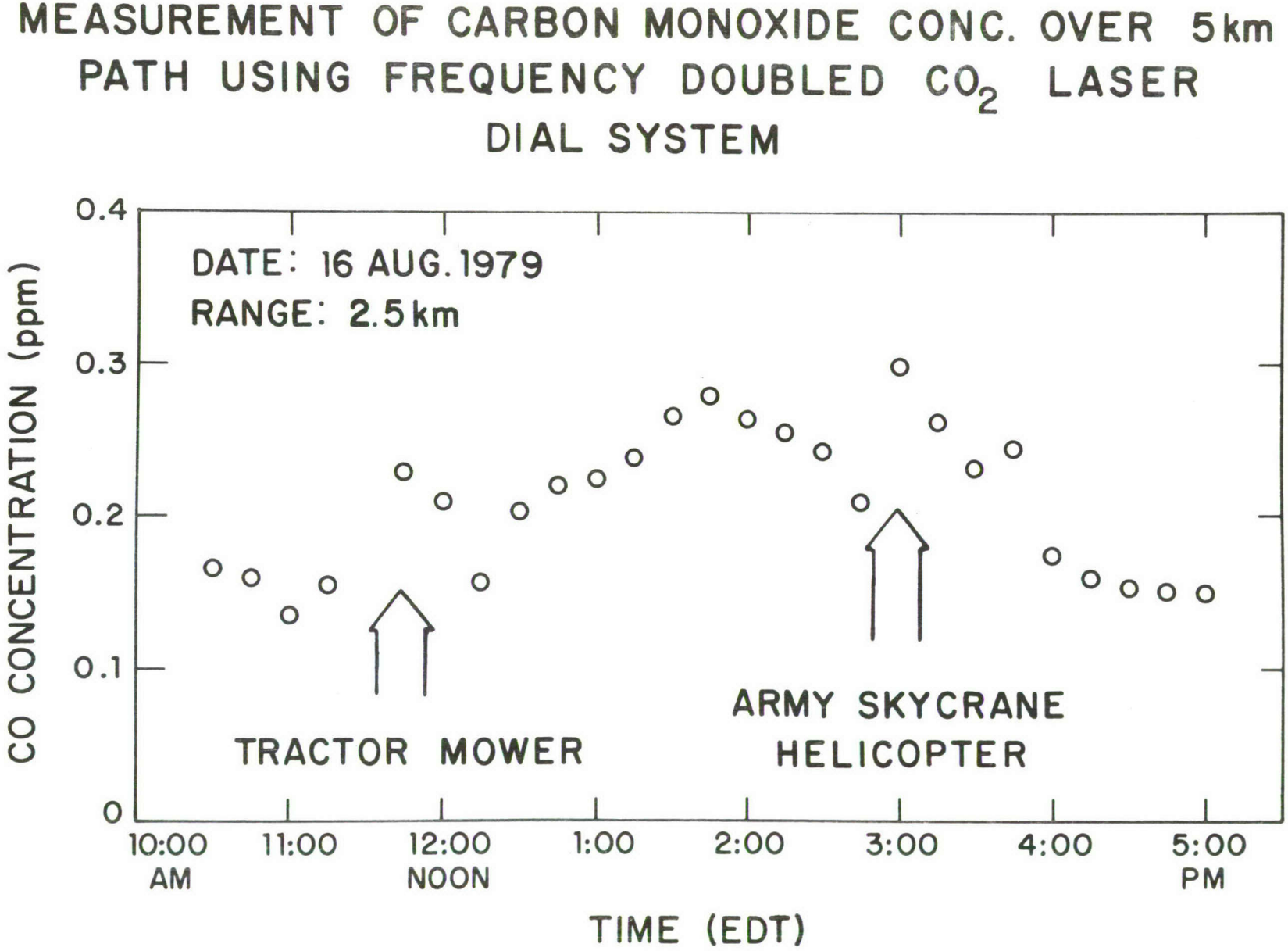
MEASUREMENT OF CARBON MONOXIDE CONC. OVER 5km PATH USING FREQUENCY DOUBLED CO_2 LASER DIAL SYSTEM
DATE: 16 AUG. 1979
RANGE: 2.5km
CO CONCENTRATION (ppm)
0.4
0.3
0.2
0.1
0
TRACTOR MOWER
ARMY SKYCRANE HELICOPTER
10:00 AM
11:00
12:00 NOON
1:00
2:00
3:00
4:00
5:00 PM
TIME (EDT)

Fig. 2.

Appendix A

The following is a preprint of a journal article to be published in Review of Scientific Instruments, February, 1980 titled "Development of a High Repetition Rate Mini-TEA CO_2 Laser".

DEVELOPMENT OF A HIGH REPETITION RATE MINI-TEA CO_2 LASER*

N. Menyuk and P. F. Moulton
Lincoln Laboratory, Massachusetts Institute of Technology
Lexington, Massachusetts 02173

Abstract

A 1.8 cm^3 active volume gas-recirculating mini-TEA CO_2 laser of relatively simple design is described. The laser is capable of operating at 500 Hz with an average output of 10 W. The device is line tunable over $\sim$ 50 CO_2 laser frequencies, has operated with up to 34 J/ℓ output density and has a nearly diffraction-limited output.

---

*This work was sponsored by the Department of the Air Force.

(Preprint of article to appear in Review of Scientific Instruments, February, 1980.)

DEVELOPMENT OF A HIGH REPETITION RATE MINI-TEA CO_2 LASER*

N. Menyuk and P. F. Moulton
Lincoln Laboratory, Massachusetts Institute of Technology
Lexington, Massachusetts 02173

I. Introduction

Typical commercially available pulsed CO_2 TEA (Transversely Excited Atmospheric) lasers operate with output energies in the 1 J and higher range. Pulse repetition rates of a few hundred Hz are available at that energy level, but the devices are by necessity large and expensive. Certain applications of TEA lasers, such as rangefinding,[1] remote sensing of gases[2] and nonlinear spectroscopy need not require such a high energy output, but do require some combination of small size, high repetition rate and line tunability.

Several investigations into scaling down the size of TEA lasers have been performed. Research motivated by the desire for a portable rangefinding device[1] has been largely devoted to minimizing laser-gas deterioration in sealed lasers.[3,4] These units, which have active volumes of 6-10 cm^3 have operated at low repetition rates. A mini-TEA laser with an active volume of 1.6 cm^3 was developed by Bua and Rudko.[5] Their laser employed a continuous gas feed and achieved a repetition rate of 100 Hz operating at a fixed frequency. Their results were particularly significant in that the mini-TEA laser developed an output energy density (> 20 J/ℓ) similar to that obtained in large devices.

The mini-TEA CO_2 laser described in this paper is a relatively simple and inexpensive gas-recirculating unit which is capable of operating at a 500 Hz repetition rate with an average power output of 10 W. The device is line-tunable over 50 CO_2 laser frequencies, operates with up to 34 J/ℓ output energy density and has an output that is nearly diffraction-limited

The laser construction is described in the next section, followed by a discussion of laser performance and finally by an enumeration of applications for which the unit has been found useful.

---

*This work was sponsored by the Department of the Air Force.

II. Laser Construction

a) Main Discharge Region

The unit containing the active volume of the laser, shown in Fig. 1, consists of two aluminum tooling plates 2.5 cm wide separated by vespel spacers. The aluminum plates support the main electrodes, which are also of aluminum, have a Rogowski profile and are bead blasted after machining to eliminate any sharp edges. The active discharge volume between the electrodes is approximately 1.8 cm^3 (4 mm x 4 mm x 110 mm). The laser beam passes through commercial O-ring fittings which allow easy insertion or removal of Brewster windows (NaCl or ZnSe) mounted on 1.25 cm diameter tubing.

The laser incorporates a UV-preionization system which consists of a row of series-connected spark gaps in the median plane parallel to the Rogowski electrodes. The spark-gap assembly (Fig. 2) consists of two ceramic bars separated at their ends by spacers which also serve as electrical connections to the outermost gaps. The bars are copper plated in a manner which allows solder-mounting of 12 pins. The design presents a minimal impedance to the gas flow, which is transverse to both the discharge direction and the laser beam.

UV preionization is further enhanced by adding a trace of the low-ionization potential seed gas tri-n-propylamine to the laser gas mixture.[6] The use of the seed gas increases the electron density in the gas mixture before the main discharge occurs.[7] It also results, in preionization, in a single ionizing process rather than a multi-photon process, which leads to a marked reduction in the minimum permissible time span between the preionization and main-electrode firings[8] and permits a simplification of the electrical circuitry by eliminating the need for a time delay of the order of microseconds. The circuit used, given in Fig. 3, places the preionizer electrodes with their doorknob-capacitor discharge supply directly in parallel with the main electrodes. The small required delay is obtained by setting the gaps to a sufficiently small value (0.25 mm) so that they

fire at a lower voltage than the main electrodes. The resultant delay is approximately 30 nanoseconds, which reduces as the spark-pin electrodes are eroded by successive firings. Before the time delay reaches zero, after $\sim 5 \times 10^7$ pulses, significant arcing between the main electrodes is observed and the preionizer electrodes must be regapped. This is accomplished simply by replacing the original spacers by a thinner set.

b) Electronic Circuit

The laser discharge circuit (Fig. 3) is basically an LC inversion generator[9] first used for CO_2 TEA lasers by Chang and Wood.[10] Reactive charging of the storage capacitors with series-connected diodes results in efficient electrical operation in the charging cycle. During repetitive pulsing the capacitors are charged to nearly twice the supply voltage. In addition to the voltage-doubling effect of resonant charging, the laser discharge circuit can also act as a voltage doubler, in that the cathode voltage swings from an initial positive value to a nearly equal negative voltage.[10] However, we observe that the main discharge fires before the full cathode voltage swing occurs, and that sets the anode-to-cathode voltage limit. Under typical operating conditions the maximum anode-to-cathode voltage during the discharge cycle is approximately twice the dc power supply voltage.

c) Gas Circulation System

For high repetition rates in a TEA laser, all the gases involved must be removed from the active volume before the onset of the succeeding pulse. Since this includes removal of the laser gas residue blown upstream by the shock wave of the previous pulse, the ratio of the distance traveled by the gas per pulse to the electrode width (clearing ratio) must be significantly greater than unity.[11,12] This requirement effectively eliminates consideration of an open gas-flow system since gas usage would be at least 100-200 liters/minute at the highest repetition frequencies. At the other extreme, a sealed recirculating gas-flow system requires such complicating features as additive gases[3,13] which reduce the laser power density or catalytic conversion through either filtration[14,15] or a heated platinum wire in the system.[16] In addition, sealed systems have limited lifetimes

between gas changes ($\sim 2 \times 10^6$ pulses), which would cause frequent stoppages at high pulse repetition rates. For these reasons we have chosen to use a semi-closed gas-recirculating system in which a small fraction of the laser gases are constantly being bled off and replaced. With this arrangement the laser can operate indefinitely, and at high power densities, with a ratio of gas replacement rate to flow rate of about 1%.

Sufficient gas circulation for a pulse repetition frequency in excess of 500 Hz can be obtained using a 3-inch fan and a small wind tunnel. The nature of the wind tunnel is flexible, and two relatively simple ones were constructed which provided homogeneous gas circulation to the laser-body unit. The first, shown in Fig. 4a, is built of standard 10 cm and 5 cm diameter plastic plumbing parts and two plexiglass units, which act as transition sections between the plastic tubing and laser body by changing the shape of the wind-tunnel cross section while maintaining a constant cross-sectional area. The fan and a water-cooled heat exchanger are contained within the 10 cm diameter section. The second recirculating system, shown in Fig. 4b, consists of two plexiglass semi-cylinders of equal length placed non-concentrically on each side of the laser so that their spacing at the top is equal to the laser interelectrode distance and the spacing at the bottom is large enough to hold the fan and heat exchanger. Short constant-area spacers are placed between the semi-cylinders and the laser body and act as stilling sections to reduce turbulence in the active region.

III. Laser Operation and Characteristic

The lasers are normally operated with a 50 cm spacing between mirrors, and most experiments have been conducted using a 15%-transmitting output coupler mirror. We have used ZnSe mirrors exclusively after finding that germanium mirrors, in the absence of external cooling, were damaged at pulse repetition rates as low as 10-20 Hz.

Optimum performance was obtained with laser-gas mixtures containing much less helium than the frequently quoted 1:1:8 ratio of CO_2:N_2:He. Our mixtures generally contained about 1/3 CO_2, slightly more N_2 and the remainder a mixture of helium, hydrogen and a small quantity of seed gas.

The addition of hydrogen led to notable performance improvement.[17] Obtaining arc-free discharges at these increased CO_2 concentrations enabled us to achieve high pulse energy densities in the system.

We have operated at dc power supply voltages between 6 and 9.5 kV. As mentioned above, the maximum anode-cathode voltage during discharge is approximately double the supply voltage, which corresponds to E/p values up to 62 V $Torr^{-1}$ cm^{-1}. The power output increases linearly with pulse-repetition frequency for a fixed supply voltage, but the highest permissible voltages at low frequencies cannot be maintained to the highest repetition rates without considerable arcing. The voltage limitation may be due to inherent plasma instabilities at the high energy densities in the active volume or, alternatively, to the need for a greater clearing ratio at the higher voltage.[11]

These aspects are illustrated in Table I. The results were obtained using a high-reflectivity (R = 99.4%) mirror in conjunction with the 85% output mirror. The laser radiation was on the P(20) line of the 10.6 μm band. At low frequencies the CO_2:N_2:He:H_2 gas ratio was 1.0:1.2:0.4:0.2; at the higher frequencies the ratio was 1.0:1.2:0.7:0.1. The 60 mJ output corresponds to an output energy density of 34 J/ℓ while the result at 503 Hz corresponds to an average output power level near 6 kW/ℓ. As indicated in Fig. 5, the output energy per pulse varies approximately linearly with the dc supply voltage over a major segment of the operating range.

The mini-TEA laser radiation is in low-order transverse modes because the small active cross-sectional area (4 x 4 mm) of the laser is comparable to the TEM_{00} cavity mode area. The mode quality is maintained at high repetition rates by the removal of the discharge gases between pulses. The TEM_{10} appears to be the dominant mode at the highest output levels, and about half the laser power is available in the TEM_{00} mode using intracavity apertures. The pulse width in the gain-switched spike of a typical pulse, shown in Fig. 6, is approximately 100 ns FWHM, with about 30-40% of the total energy contained in the tail section.

The ability to tune among various CO_2 transitions is essential for some applications, such as atmospheric monitoring. However, we found that simple replacement of the high reflectivity mirror with a grating in our

laser led to a significant loss of laser efficiency and, more importantly, optical damage to the grating. Both problems were resolved by using a three-mirror cavity in which a partially reflecting mirror is placed between the Littrow-mounted grating and the active medium to form, with the grating, a tunable reflector with a higher reflectivity than that of the grating alone.[18,19] We employed a 63%-reflecting ZnSe mirror in our three-mirror cavity. The effect of the reflector in the system, for a grating reflectivity of 85 to 90%, is to increase the effective grating reflectivity to 98% while simultaneously decreasing the radiation intensity at the grating by a factor of eight.[18] Laser output in the strongest lines increased by 20% compared with operation in the conventional cavity without the 63% reflector, and grating damage was eliminated. Single-line laser radiation was obtained on about 50 lines, from the P(8) to P(36) and the R(10) to R(34) lines of the (00°1) - (10°0) transition and from the P(10) to P(34) and the R(10) to R(34) lines of the (00°1) - (02°0) transition.

IV. Applications

Its versatility, good mode quality, high-repetition rate with high-average power capability and tunability have already led to widely varied applications of the mini-TEA laser within the Laboratory. The good mode quality of the laser is particularly important for high efficiency in frequency-conversion applications. The highest average power second harmonic conversion efficiency reported to date for CO_2 laser-frequency doubling, over 28.5%, was achieved using the mini-TEA laser to pump a $CdGeAs_2$ crystal. The mini-TEA was also used as the fundamental frequency source in a frequency-tripling experiment which yielded a peak-power conversion efficiency near 6%.[21] The mini-TEA laser has also served as the pulse section of a hybrid laser in conjunction with a low-pressure gain cell in the optical cavity. This use was for a study of the double-resonance spectroscopy of SF_6,[22] which required a single-frequency laser operating at a relatively high repetition rate. In this mode of operation, which was carried out for several weeks, the laser generated an energy of 8 mJ on a single frequency operating at 80 Hz PRF for several hours each

day. The laser is currently being used in conjunction with a frequency-doubling crystal as the primary coherent radiation source of a differential absorption LIDAR system. The tuning capability at high repetition rates of the mini-TEA laser, coupled with efficient frequency doubling makes this system particularly effective for monitoring the presence of CO^{23} and several other species having absorption lines in the 5 and 10 μm wavelength region.

Acknowledgments

We want to express our thanks to Dr. A. Mooradian for his overall support and encouragement. We are also indebted to E. J. Casazza, W. E. DeFeo, H. R. Favreau and B. Feldman for their technical support on various phases of the laser development.

Table I. Mini-TEA Laser Power and Energy Output

D.C. Power Supply Voltage (kV)	Pulse Repetition Frequency (Hz)	Average Power Output (W)	Energy per Pulse (mJ)
a) $CO_2:N_2:He:H_2$ = 1:1.2:0.4:0.2			
9.4	33	2	60.6
9.4	51	3	59
8.5	100	5	50
8.6	149	7.5	50.3
8.3	208	9.2	44.2
b) $CO_2:N_2:He:H_2$ = 1:1.2:0.7:0.1			
7.4	420	10	23.8
6.65	450	10	22.2
6.55	503	10.5	20.5

REFERENCES

1. M. J. Taylor, P. H. Davies, D. W. Brown, W. F. Woods, I. D. Bell and C. J. Kennedy, Appl. Opt. 17, 885 (1978).
2. R. T. H. Collis, Appl. Opt. 9, 1782 (1970).
3. B. Norris and A. L. S. Smith, Appl. Phys. Lett. 34, 385 (1979).
4. D. S. Stark and M. R. Harris, J. Phys. E: Sci. Instrum. 11, 316 (1978).
5. D. P. Bua and R. I. Rudko, IEEE/OSA Conference on Laser Engineering and Applications, Washington, D.C., (1977), Paper 6.9.
6. J. S. Levine and A. Javan, Appl. Phys. Lett. 22, 55 (1973).
7. A. Javan and J. S. Levine, IEEE J. Quantum Electron. QE-8, 827 (1972).
8. B. J. Reits and A. H. M. Olbertz, Appl. Phys. Lett. 26, 335 (1975).
9. R. A. Fitch, IEEE Trans. Nucl. Sci. NS-18, 190 (1971).
10. T. Y. Chang and O. R. Wood, IEEE J. Quantum Electron. QE-8, 721 (1972).
11. G. S. Dzakowic and S. A. Wutzke, J. Appl. Phys. 44, 5061 (1973).
12. V. Yu. Baranov, V. V. Breev, D. D. Malyuta and V. G. Niz'ev, Sov. J. Quantum Electron. 7, 1059 (1977).
13. P. W. Pace and M. Lacombe, IEEE J. Quantum Electron. QE-14, 263 (1978).
14. C. Willis, R. A. Buck and J. G. Purdon, Appl. Phys. Lett. 31, 84 (1977).
15. R. B. Gibson, A. Javan and K. Boyer, Appl. Phys. Lett. 32, 726 (1978).
16. D. S. Stark, P. H. Cross and M. R. Harris, J. Phys. E:Sci. Instrum. 11, 311 (1978).
17. T. F. Deutsch, Appl. Phys. Lett. 20, 315 (1972).
18. J. E. Bjorkholm, T. C. Damen and J. Shah, Opt. Commun. 4, 283 (1971).

19. G. J. Ernstand and W. J. Witteman, IEEE J. Quantum Electron. QE-7, 484 (1971).
20. N. Menyuk, G. W. Iseler and A. Mooradian, Appl. Phys. Lett. 29, 422 (1976).
21. N. Menyuk and G. W. Iseler, Opt. Lett. 4, 55 (1979).
22. P. Moulton and A. Mooradian (to be published).
23. D. K. Killinger and N. Menyuk, J. Opt. Soc. Am. 69, 1398 (1979).

FIGURE CAPTIONS

Fig. 1. Active discharge section of mini-TEA laser.

Fig. 2. UV preionizer assembly for mini-TEA laser.

Fig. 3. Mini-TEA laser discharge circuit including UV preionization.

Fig. 4. High-repetition-rate circulating gas-flow mini-TEA CO_2-laser systems: a) tubular unit; b) cylindrical unit.

Fig. 5. Output pulse energy as a function of dc power supply voltage at PRF = 206 Hz.

Fig. 6. Typical mini-TEA CO_2-laser output pulse.

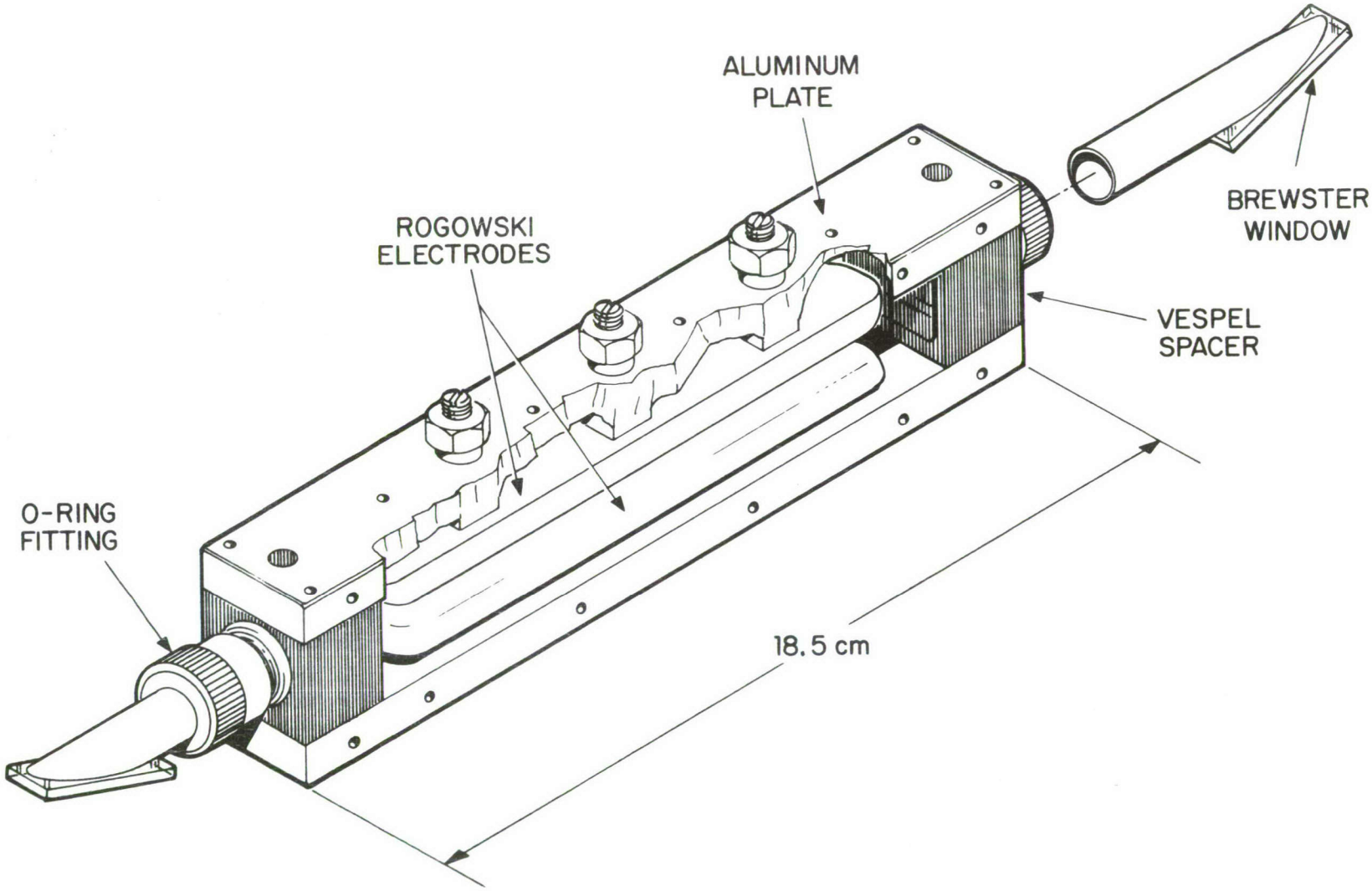
ALUMINUM
PLATE
BREWSTER
WINDOW
ROGOWSKI
ELECTRODES
VESPEL
SPACER
O-RING
FITTING
18.5 cm

Fig. 1

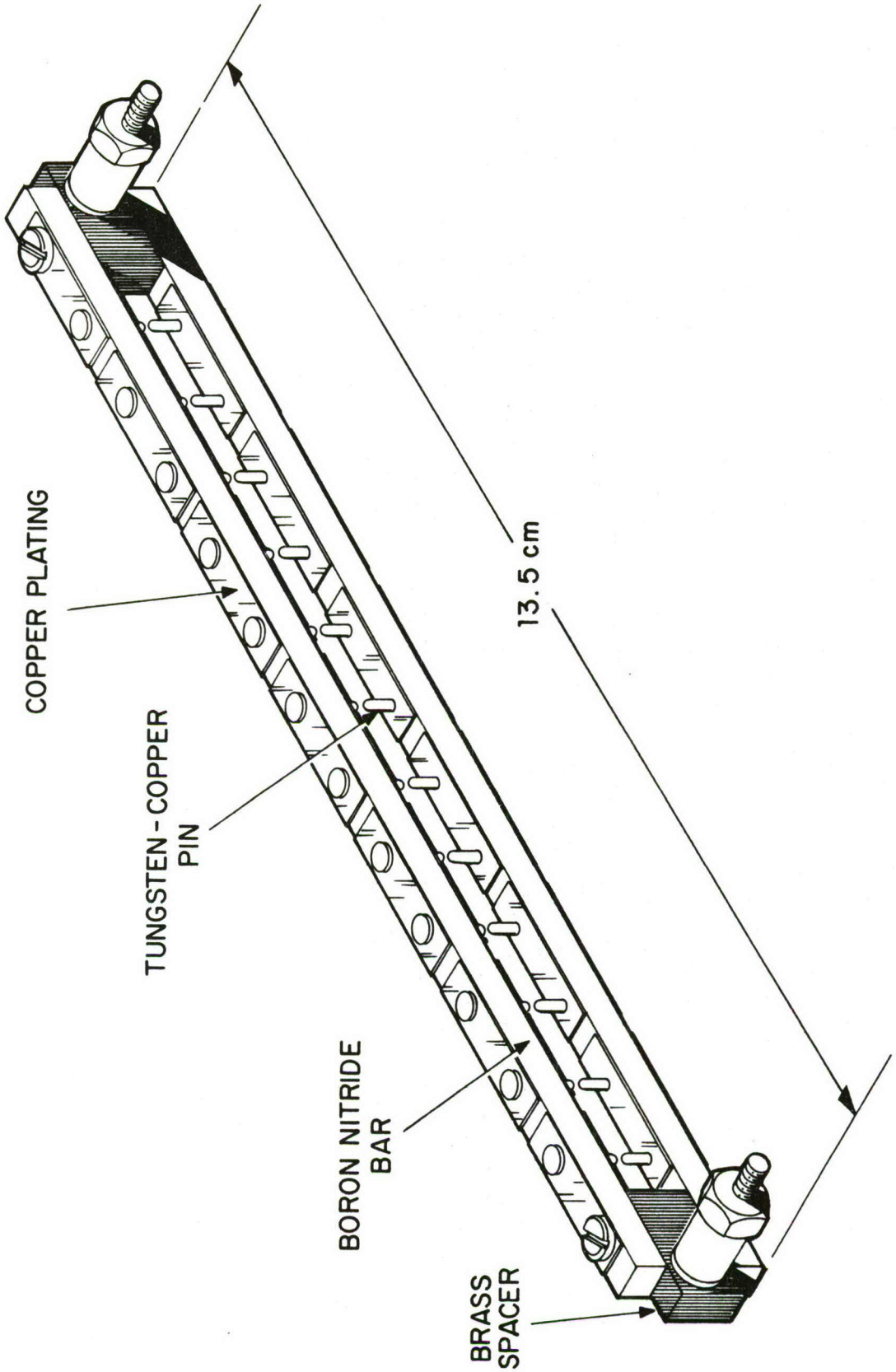
COPPER PLATING
TUNGSTEN - COPPER PIN
BORON NITRIDE BAR
BRASS SPACER
13.5 cm

Fig. 2

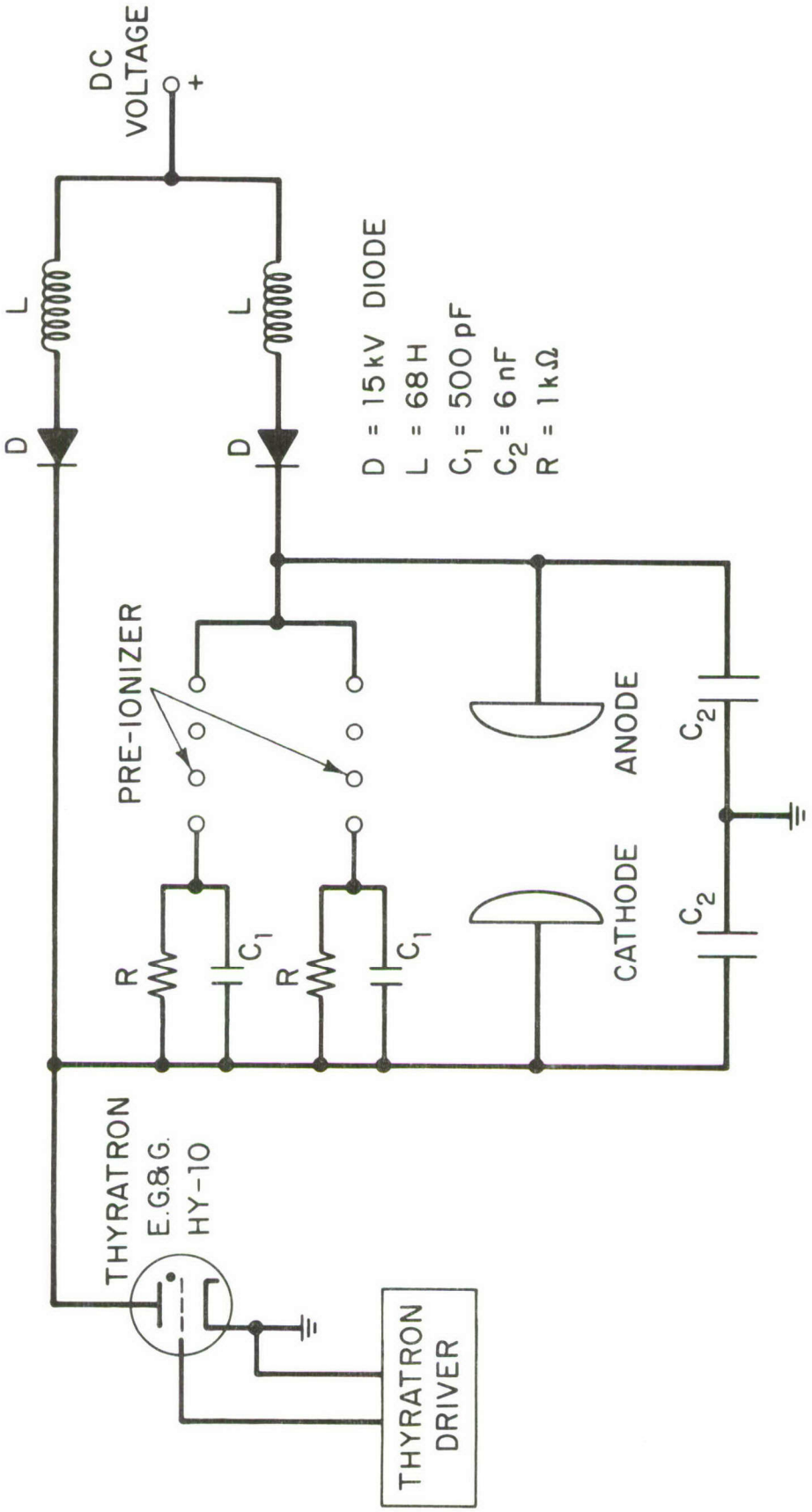
DC
VOLTAGE
+
L
L
D
D
D = 15 kV DIODE
L = 68 H
C_1 = 500 pF
C_2 = 6 nF
R = 1 kΩ
PRE-IONIZER
R
C_1
R
C_1
CATHODE
ANODE
C_2
C_2
THYRATRON
E.G.&G.
HY-10
THYRATRON
DRIVER

Fig. 3

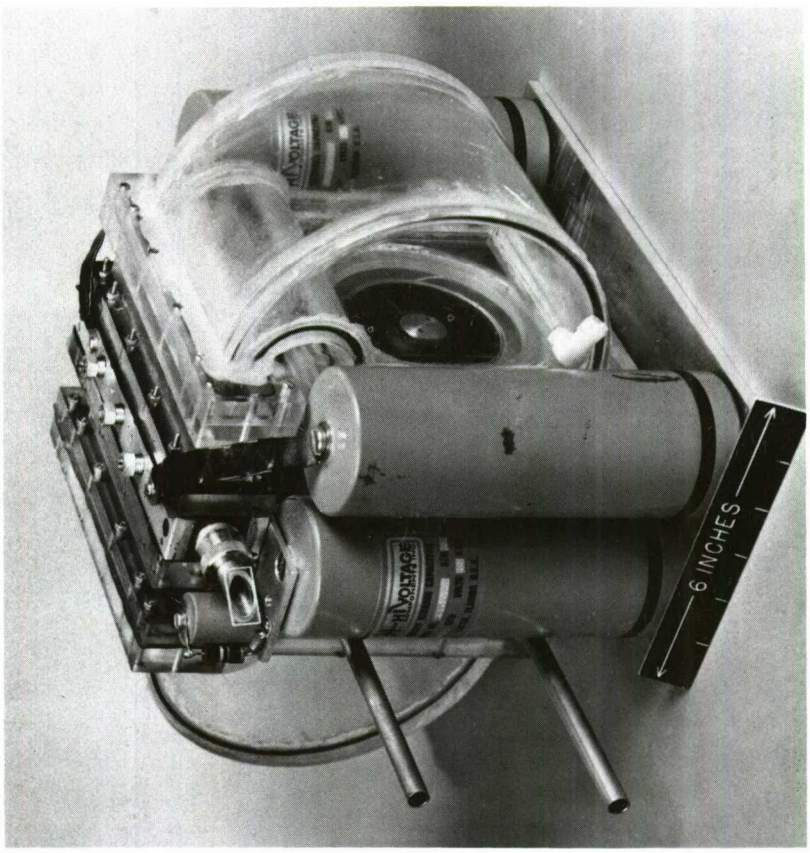

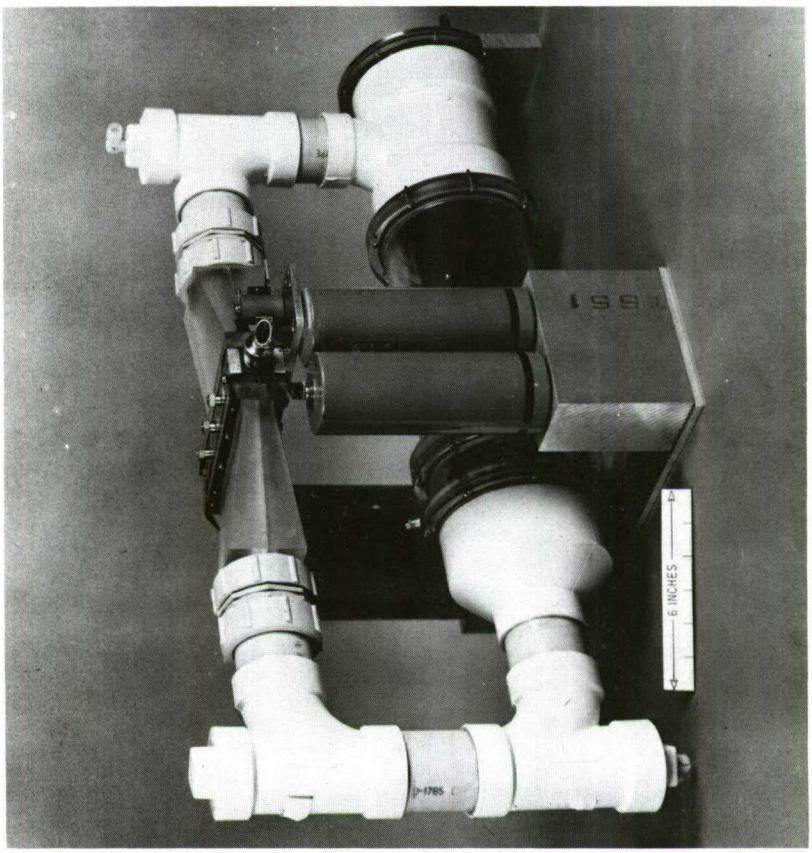

Fig. 4

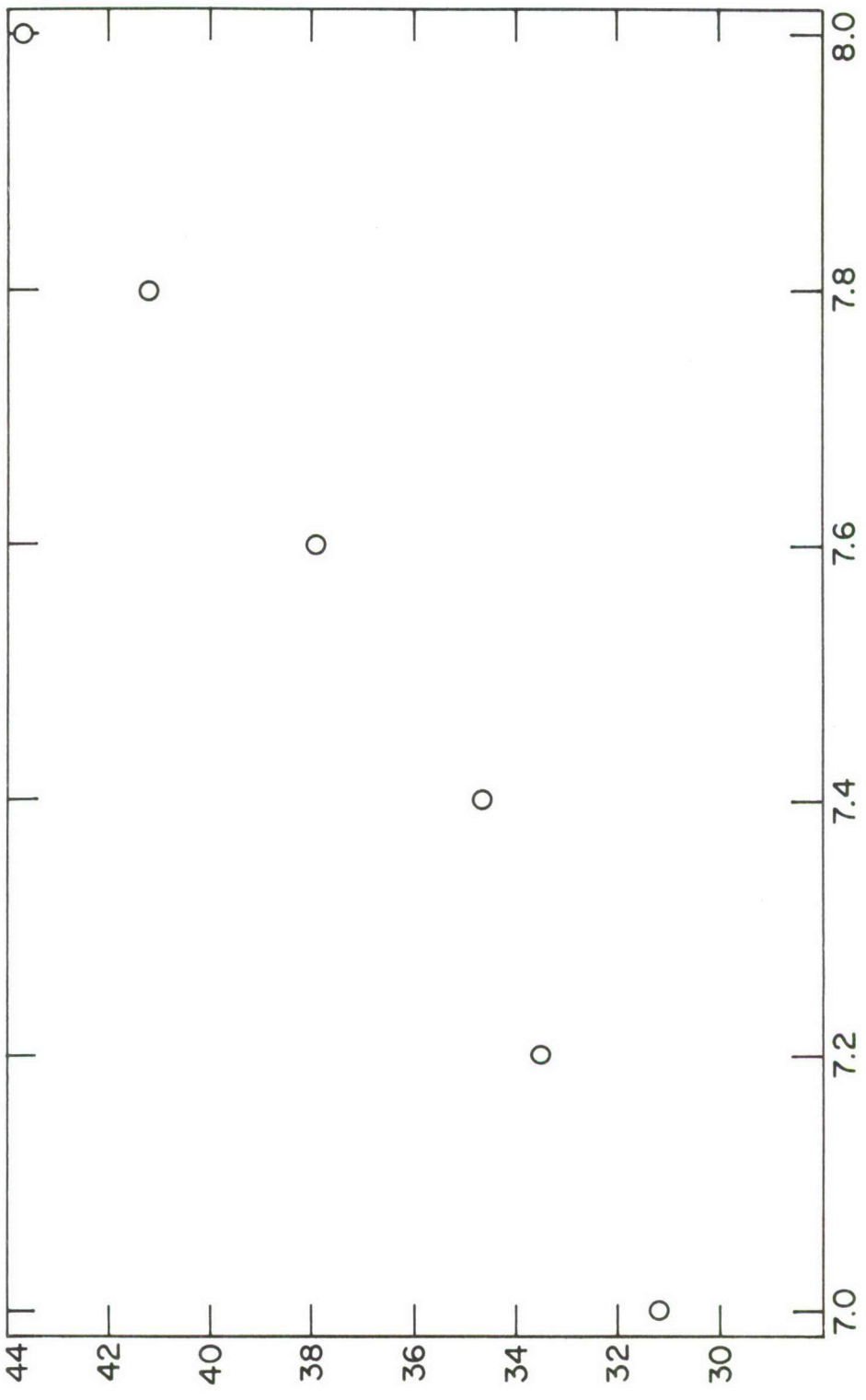
OUTPUT PULSE ENERGY (mJ)
44
42
40
38
36
34
32
30
7.0
7.2
7.4
7.6
7.8
8.0
DC POWER SUPPLY VOLTAGE (kV)

Fig. 5

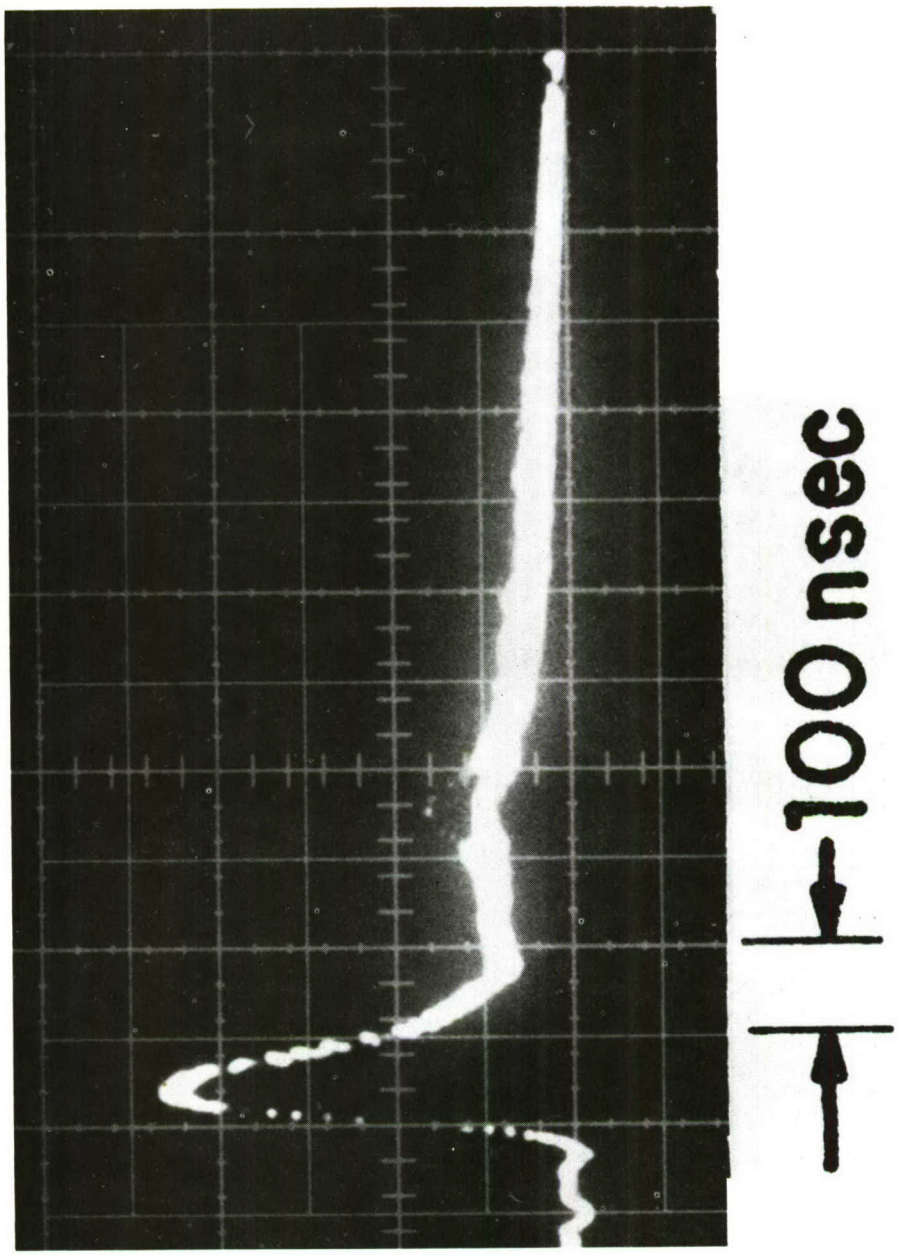

Fig. 6

Appendix B

The following is a reprint of an internal Lincoln Laboratory memorandum titled "Preferred Frequencies for Remote Sensing of CO and NO".

MASSACHUSETTS INSTITUTE OF TECHNOLOGY
LINCOLN LABORATORY

21 December 1978

TO: A. Mooradian and P. L. Kelley

FROM: N. Menyuk

SUBJECT: Preferred Frequencies for Remote Sensing of CO and NO

Introduction

This memorandum has as its main purpose the determination of the best frequencies to be used for remote sensing of NO and CO using the frequency coincidences of the absorption lines of these molecules with frequency-doubled radiation from a CO_2 mini-TEA laser. Where appropriate, it also considers the advantages to be gained using sum generation of CO_2 laser radiation instead of frequency doubling. The study involved consideration of the limitations of the primary source and the atmospheric attenuation at the available frequency coincidences. Recommendations are given in the summary and conclusions section of this memo; the basis for these recommendations form the body of the report.

Remote Sensing Coincidences

The use of frequency-doubled CO_2 laser radiation for remote sensing of NO and CO molecules in the effluence of moving vehicles is limited to those CO_2 laser lines whose doubled frequency coincides with an absorption line of the molecules. In this context, coincidence is defined as a frequency difference $\Delta\nu < 0.1\ cm^{-1}$. All such coincidences between the 1-0 absorption bands of CO and NO and frequency doubled $^{12}C^{16}O_2$ laser lines are listed in Table I.

However, several of the lines in Table I will not be suitable for our use, either because the coincidence is with a line having low molecular absorption or because the line is unobtainable with the mini-TEA laser. These factors combine to eliminate the R(8) and R(30) lines of the $(00^{o}1)$ - $(02^{o}0)$ band and the

R(42), R(40) and R(8) lines of the $(00^{o}1)$ - $(10^{o}0)$ band. Thus we are left with two possible laser lines coincident with CO, namely R(18) and P(24) of the $(00^{o}1)$ - $(02^{o}0)$ band and three lines coincident with NO, namely R(22), P(24) and P(8) of the $(00^{o}1)$ - $(10^{o}0)$ band. Of these, the P(8) is only marginally obtainable with the mini-TEA laser.

We have investigated the atmospheric absorption characteristic of these five frequencies and for the two CO_2 laser frequencies nearest each of them. The computer program used in this investigation employed the AFCRL absorption line compilation.[1] The transmission predicted for each of the 15 frequencies over a horizontal path at ground level for a 2 km range (4 km including return) is given in Table II for both the midlatitude winter and midlatitude summer atmospheric models. A 5 km visibility was assumed. A zero in either relative transmission column corresponds to $I/I_o < 10^{-6}$.

The results given in Table II indicate that while the coincidences of frequency-doubled CO_2 laser lines with absorption peaks of CO occur in regions of fairly high atmospheric transmission, the same is not true for the coincidences with NO. Therefore, we will consider each of the molecules separately.

1) Carbon Monoxide (CO)

Both CO-doubled CO_2 coincidences considered in Table II occur at frequencies with sufficient atmospheric transmission to be useful. The transmission at the coincident frequencies is significantly lower than at the neighboring frequencies, except for the P(22). This is to be expected since the CO present in the atmosphere is the major source of absorption at coincidence. The relatively minor role played by water vapor is indicated by comparison of the midlatitude summer and winter columns; the summer column corresponds to a four-fold increase in atmospheric water vapor. This is not the situation for the exceptional case, namely the frequency corresponding to the doubled P(22) CO_2 laser

line of the $(10^{o}0)$ - $(02^{o}0)$ band. This frequency lies within .05 cm^{-1} of two moderately strong water vapor lines, which results in almost total absorption of the laser radiation.

In a differential absorption arrangement, the P(26) line can be used in conjunction with the P(24) line. Alternatively, either the R(16) or R(20) can be used in conjunction with the R(18) coincidence. On the basis of Table II alone, the use of either the P(24) or R(18) as the coincident line are virtually equivalent; however, the mini-TEA laser radiation is over 50% greater at the P(24) frequency. Hence, it is the frequency of choice.

Since atmospheric CO is the major cause of radiation absorption at coincidence, it limits the remote sensing range. The variation of atmospheric transmission with range at the P(24) and P(26) frequencies are shown in Fig. 1 for midlatitude atmospheric models. It is possible to remotely sense the presence of pockets of CO at greater ranges than is available with the doubled P(24) by using coincidences which are not as close as that which occurs with the P(24) (where $\Delta\nu = .0042\ cm^{-1}$).[2] The R(18) coincidence is also very close and, as seen in Table II, has an even lower transmission. To achieve a significant increase in range, it will be necessary to use sum generation in place of frequency doubling.

2) Nitric Oxide (NO)

The overlap of the fundamental 1-0 absorption band of nitric oxide with doubled CO_2 laser radiation lies roughly in the frequency range between 1860 and 1980 cm^{-1}. This is also a range in which water vapor absorption is extremely high and, in fact, renders most of the region unsuitable for remote sensing purposes. There are, however, a number of narrow frequency regions which can be considered small "windows" where, at midlatitude water vapor levels, atmospheric absorption is relatively low.[3] The P(24) and P(26) lines of

the $(10^{o}0)$ - $(00^{o}1)$ band lie in such a window; in fact, in the only such "window" below 1898 cm^{-1}. The R(20) line near 1952 cm^{-1} lies in a similar window. Even in these "window" regions, the tails of neighboring water vapor lines are still the major source of radiation absorption. This is evident from a comparison of the winter and summer midlatitude transmission.

For remote sensing via frequency doubling of a mini-TEA laser, Table II indicates that the P(24) line of the $(10^{o}0)$ - $(00^{o}1)$ band is the only usable coincidence line. The table also indicates that the range is restricted by water vapor effects and that the restriction is severe under high humidity conditions. The relative transmission vs range for a midlatitude atmospheres at the P(24) and P(26) frequencies are given in Fig. 2.

Given this limitation, it is worthwhile to consider the possibility of using mini-TEA lasers for sum generation instead of frequency doubling. To be usable, the sum generated coincidence should arise from two frequencies that can be emitted by the mini-TEA lasers and, at the same time, must lie within one of the "windows" discussed above. This pair of qualifications eliminates most of the available coincidences. Those remaining are listed in Table III. In addition to the lines shown in the table, there are coincidences above 1972 cm^{-1} which lie in the most transparent region of the atmosphere overlapping NO. Unfortunately, this is the high angular momentum (J) region of the NO R-band spectrum, and the absorption line intensities are weak. Since the minimum detectable molecular concentration in a differential absorption arrangement is inversely proportional to the absorption line intensity, the greater range available above 1972 cm^{-1} can only be purchased at the cost of significantly reduced detection sensitivity ($\sim$ 3 orders of magnitude between ν = 1972 cm^{-1} and 1930 cm^{-1}).

The first two coincidences listed in Table III lie in the same "window" as the frequency-doubled P(24) [$(00^{o}1) - (10^{o}0)$] CO_2 laser line, and are coincident with the same NO $R(1/2)_{1/2}$ absorption line. They offer no advantage over the doubled line. The absorption line intensity of the $R(1/2)_{1/2}$ NO line, namely 0.177×10^{-19} cm^{-1}/molecule cm^{-2}, is comparable to the intensities of the NO $R(33/2)_{3/2}$ and $R(35/2)_{1/2}$ lines as given in Table III. Thus the improved atmospheric transmission obtainable with these lines using sum generation relative to frequency doubling should not involve any significant decrease in molecular detection sensitivity. However, the improvement in atmospheric transmission does not seem to be great enough to warrant the increased system complexity involved in sum generation unless and until sufficient motivation for the moderate attainable improvement is demonstrated.

Summary and Conclusions

We have found that strong frequency-doubled CO_2 laser lines coincident with a CO absorption line occur at frequencies where atmospheric absorption is low. The best laser line for our purpose, and the one recommended, is the P(24) line of the $(00^{o}1) - (02^{o}0)$ band. For differential absorption, the P(26) line is available with even less atmospheric absorption. The major absorption of the P(24) line is due to the presence of CO in the atmosphere. At some time in the future it may be desirable to increase the effective remote sensing range by having a coincidence with the CO_2 laser radiation further from the absorption line center than occurs for either of the frequency-doubled cases listed in Table I. That would be the only reason for considering the use of sum generation for remote sensing of CO, and clearly does not justify its use initially.

The only coincidence of a strong frequency-doubled CO_2 laser line and an NO absorption line that can be used is the P(24) line of the $(10^{o}0) - (00^{o}1)$ band.

The atmospheric absorption due to water vapor is high at this frequency, but the alternatives are much worse. It is therefore the recommended frequency.

Using the sum generation of the R(22) and the P(10) or P(8) lines of the $(10^{o}0)$ - $(00^{o}1)$ bands should lead to some improvement in atmospheric transmission with little or no cost in molecular detection sensitivity. Despite this, however, I still recommend using the frequency-doubled P(24) line rather than sum generation at this time. One reason for this recommendation is the fact that the P(10) and P(8) lines lie fairly far down on the CO_2 laser gain curve, resulting in reduced coherent radiation at the sum generated frequency. Another is to avoid the additional complexity of a sum-generating system until there is sufficient motivation for attempting it and until we become more familiar with other range restrictions and the extent to which they will further limit the gain due to the moderate improvement in atmospheric transmission.

Significantly greater atmospheric transmission is available by sum generation above 1972 cm^{-1}. However, the NO absorption line intensity is so low in this spectral region that the molecular detection sensitivity would be down by $\sim$ 3 orders of magnitude due to that factor alone.

I would like to acknowledge the work of Barbara Palm and thank her for her programming efforts and for supplying all the computer-based data used in this report.

REFERENCES:

1. R. A. McClatchey, R. W. Fenn, J. E. A. Selby, F. E. Volz and J. S. Garing, Optical Properties of the Atmosphere (Third Edition), Environmental Research Paper, No. 411, AFCRL-72-0497 (1972).

2. R. L. Byer and M. Garbuny, Appl. Optics 12, 1496 (1973).

3. R. J. Nordstrom, J. H. Shaw, W. R. Skinner, J. G. Calvert, W. H. Chan and W. M. Uselman, Application of Fourier Transform Spectroscopy to Air Pollution Problems, Interim Report-1976, Computer-Generated Long-Path Air Spectra, EPA-600/3-77-026 (1977).

NM:az

Table I. Spectral Coincidences Between NO and CO Absorption Lines and Frequency Doubled CO_2 Laser Radiation

Molecule	Absorption Line Identification	Absorption Line Frequency* (cm^{-1})	CO_2 Laser Line Identification	Doubled CO_2 Laser Frequency** (cm^{-1})	$\Delta\nu$ ($2\nu_{CO_2} - \nu_{mol.}$) (cm^{-1})
NO	$R(73/2)_{3/2}$	1977.2721	+R(42)	1977.29546	.0234
	$R(71/2)_{3/2}$	1975.2971	+R(40)	1975.24230	-.0548
	$R(53/2)_{1/2}$	1954.3952	+R(22)	1954.42922	.0340
	$R(37/2)_{3/2}$	1935.4951	+R(8)	1935.41584	-.0793
	$R(19/2)_{1/2}$	1909.1281	+P(8)	1909.09160	-.0365
	$R(1/2)_{1/2}$	1881.0398	+P(24)	1881.09766	.0579
CO	R(6)	2169.19834	†R(30)	2169.27032	.07198
	R(2)	2154.59598	†R(18)	2154.60498	.00900
	P(14)	2086.32231	†P(24)	2086.32650	.00419

+ - (10°0)-(00°1) Band; † - (10°0)-(02°0) Band

* - NO Frequencies from Laboratoire de Spectroscopie Moleculaire, Univ. de Paris VI, 1973 (unpublished)
CO Frequencies evaluated from Dunham coefficients given by H. Kildal, R. S. Eng and A. H. M. Ross, J. Mol. Spectrosc. 53, 479 (1974)

** - CO_2 Laser frequencies from Handbook of Lasers, R. J. Pressley, Ed., Chem. Rubber Company, Cleveland, Ohio

Table II. Atmospheric transmission for 2 km (2-way) horizontal range at ground level.

Atmosphere Model		Midlatitude Winter	Midlatitude Summer
CO_2 Line Identification	Doubled Frequency (cm^{-1})	Relative Transmission I/I_o	Relative Transmission I/I_o
$^{+}P(26)$	1877.3780	0.193	1.14×10^{-3}
$^{*+}P(24)$	1881.0977	0.262	3.09×10^{-3}
$^{+}P(22)$	1884.7682	0	0
$^{+}P(10)$	1905.7632	0.093	5.33×10^{-5}
$^{*+}P(8)$	1909.0916	9.0×10^{-6}	0
$^{+}P(6)$	1912.3714	0.062	10^{-5}
$^{+}R(20)$	1951.8622	0.577	0.091
$^{*+}R(22)$	1954.4292	0.029	0
$^{+}R(24)$	1956.9460	0.185	3.74×10^{-4}
$^{x}P(26)$	2082.5582	0.875	0.650
$^{\dagger x}P(24)$	2086.3265	0.516	0.311
$^{x}P(22)$	2090.0434	0	0
$^{x}R(16)$	2151.9756	0.914	0.723
$^{\dagger x}R(18)$	2154.6050	0.424	0.260
$^{x}R(20)$	2157.1812	0.925	0.783

$^{+}(10°0)-(00°1)$ band
$^{x}(10°0)-(02°0)$ band
*coincident line-NO
†coincident line-CO

Table III. Sum generated coincidences with NO absorption lines

CO_2 Laser Line ID (10°0)-(00°1)	Sum Generated Frequency (cm^{-1})	NO Absorption Line ID	Absorption Line Frequency (cm^{-1})	Frequency Difference Δ (cm^{-1})	NO Absorption Line (cm^{-1}/mol-cm^{-2})	Midlatitude Relative Transmission I/I_o Winter	Summer
P(20)+P(28)	1880.99778	$R(1/2)_{1/2}$	1881.0398	-.0420	$.177 \times 10^{-19}$	.257	.0032
P(22)+P(26)	1881.07159	$R(1/2)_{1/2}$	1881.0398	.0318	$.177 \times 10^{-19}$	.258	.0029
P(10)+R(22)	1930.09477	$R(33/2)_{3/2}$	1930.0538	.0410	$.119 \times 10^{-19}$	.495	.043
P(8)+R(22)	1931.75901	$R(35/2)_{1/2}$	1931.7273	.0317	$.182 \times 10^{-19}$	.362	.0093
P(8)+R(28)	1935.45830	$R(37/2)_{3/2}$	1935.4951	-.0368	$.733 \times 10^{-20}$	.081	0

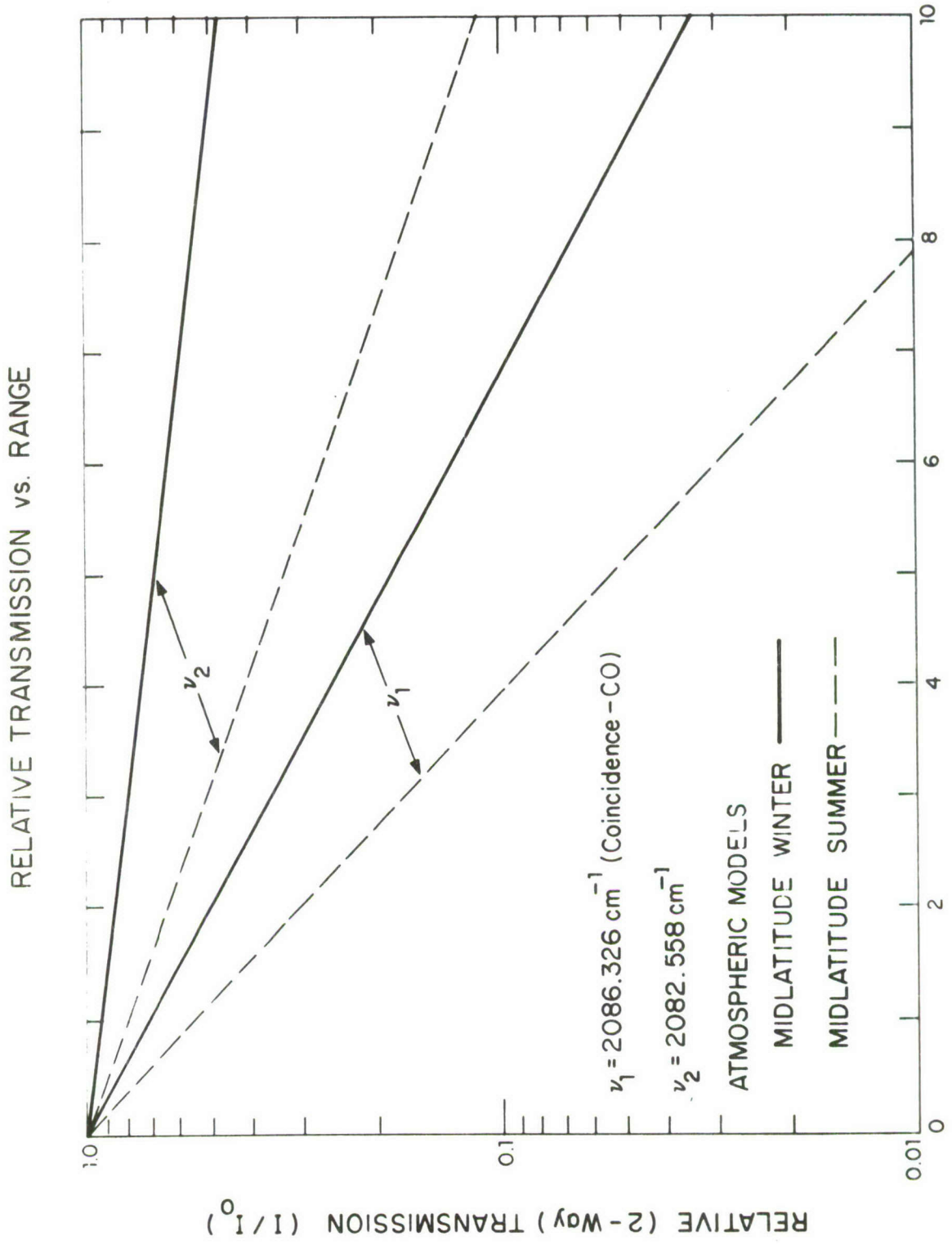
RELATIVE TRANSMISSION vs. RANGE
RELATIVE (2-Way) TRANSMISSION (I/I$_o$)
1.0
0.1
0.01
0
2
4
6
8
10
RANGE (km)
ν_2
ν_1
ν_1 = 2086.326 cm^{-1} (Coincidence-CO)
ν_2 = 2082.558 cm^{-1}
ATMOSPHERIC MODELS
MIDLATITUDE WINTER
MIDLATITUDE SUMMER

Fig. 1

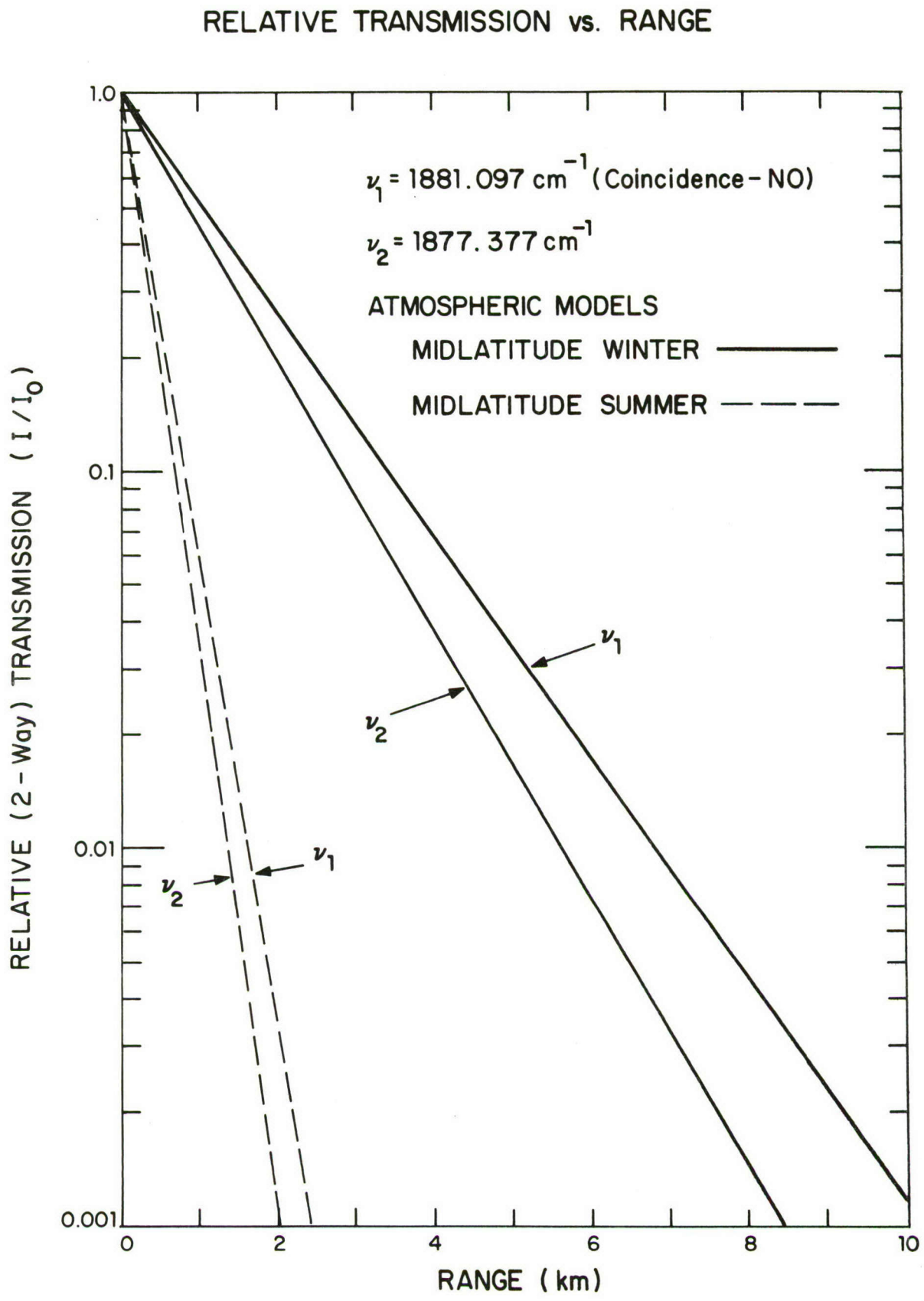
RELATIVE TRANSMISSION vs. RANGE
ν_1 = 1881.097 cm^{-1} (Coincidence - NO)
ν_2 = 1877.377 cm^{-1}
ATMOSPHERIC MODELS
MIDLATITUDE WINTER
MIDLATITUDE SUMMER
ν_1
ν_2
ν_1
ν_2
RELATIVE (2-Way) TRANSMISSION (I/I$_0$)
1.0
0.1
0.01
0.001
0
2
4
6
8
10
RANGE (km)

Fig. 2

Appendix C

The following is a reprint of an internal Lincoln Laboratory memorandum titled "Possible Frequencies for the Remote Sensing of C_2H_4, NH_3, O_3, and CH_3OH".

MASSACHUSETTS INSTITUTE OF TECHNOLOGY
LINCOLN LABORATORY
5 January 1979

TO: A. Mooradian and P. L. Kelley

FROM: N. Menyuk

SUBJECT: Possible Frequencies for Remote Sensing of Ethylene, Ammonia, Ozone and Methanol

Although the mini-TEA CO_2 laser is to be used in a frequency-doubled mode with $CdGeAs_2$ for the remote sensing of CO and NO, it can clearly be used directly as the primary radiation source for the detection of other gases with coincident spectra in the 9.2-10.8 μm region.

Studies have been made[1,2] of several important gases which fall into this category, namely ethylene (C_2H_4), ammonia (NH_3), ozone (O_3) and methyl alcohol or methane (CH_3OH). Hanst[1] measured the absorption spectra of all these gases, with the results shown in Figs. 1 and 2. He also specified the CO_2 laser lines best suited for remote sensing purposes on the basis of his results. Patty et al.,[2] using a CO_2 laser source, determined the absorption coefficients of C_2H_4, NH_3 and O_3 for each of the laser lines of both the 9.4 and 10.4 μm branches. His results are given in Table I.

Recommendations regarding the CO_2 laser lines to be used for the remote sensing of each of these gases is given below. The recommended lines are attainable with a mini-TEA laser. We have used the AFCRL absorption line compilation[3] to determine the predicted relative transmission, I/I_o, for each of the recommended lines over a 2-way, 2 km range at ground level assuming a 5 km visibility for both midlatitude winter and midlatitude summer atmospheres. The results are given in Table II. The effect of the added water vapor in the midlatitude summer atmosphere is seen to be significant. The increased absorption is almost entirely due to the H_2O absorption continuum, which plays an important role in this spectral region. The effect of individual H_2O line absorption is relatively minor. Our conclusions, which are discussed for each of the gases in turn, are essentially in accord with those of Hanst.[1]

1) Ethylene (C_2H_4)

The results of both Hanst and Patty et al. show the P(14) line of the $(00^0 1)$-$(10^0 0)$ band, which falls in the Q-branch of the ethylene absorption band, to have by far the highest absorption coefficient. It is therefore the "on-coincidence" line of choice. The neighboring P(16) and P(12) laser lines have ethylene absorption coefficients which are low compared with the P(14), but which are high relative to most other lines. Therefore, if one of these is used as the "off-coincidence" line, it will be necessary to calibrate for the significant ethylene absorption in either line. Between using the P(12) or the P(16) as the "off-coincidence" line, the P(16) is the preferred choice because the mini-TEA laser output is ~ 15-20% greater on this line. However, if a non-adjacent line can be used for "off-coincidence", the P(22) laser line has one fourth the ethylene absorption of either the P(12) or P(16) and would be preferable.

2) Ammonia (NH_3)

The CO_2 laser line which has the highest ammonia absorption coefficient and which can be emitted by the mini-TEA laser is the P(32) line of the $(00^0 1)$-$(10^0 0)$ band. It is the recommended "on-coincidence" line. The adjacent P(30) ammonia absorption coefficient is down by a factor of 20 and is the choice for the "off-coincidence" line.

3) Ozone (O_3)

The P(26) CO_2 laser line of the $(00^0 1)$-$(02^0 0)$ band has a high ozone absorption coefficient and is adjacent to the P(24) line which has a very low ozone absorption. They are therefore the choices for on- and off-coincidence respectively. The transmission of the P(26) indicates that normal ozone levels in the atmosphere at ground level will not be a serious restriction over limited ranges (2 km in our example).

4) Methyl Alcohol or Methanol (CH_3OH)

High methanol absorption is obtained using the P(32) CO_2 laser line of the $(00^0 1)$-$(02^0 0)$ band, while the methanol absorption of the P(30) line is relatively low.

Summary and Conclusions

All the gases considered are good candidates for remote sensing by differential absorption with the mini-TEA laser as the primary radiation source. The laser line choices for "on-coincidence" and "off-coincidence" absorption are summarized in Table III.

NM:az

References:

1. P. L. Hanst, "Spectroscopic Methods for Air Pollution Measurement" in Advances in Environmental Science and Technology, Vol. 2, J. N. Pitts, Jr. and R. L. Metcalf, Eds., (Wiley-Interscience, 1971).

2. R. R. Patty, G. M. Russwurm, W. A. McClenny and D. R. Morgan, Appl. Optics 13, 2850 (1974).

3. R. A. McClatchey, R. W. Fenn, J. E. A. Selby, F. E. Volz and J. S. Garing, Optical Properties of the Atmosphere (Third Edition), Environmental Research Paper, No. 411, AFCRL-72-0497 (1972).

*Table I. Absorption Coefficients $(atm\text{-}cm)^{-1}$[300 K]

Spectral line	00°1–02°0 band				00°1–10°0 band		
	μm (air)	NH_3	C_2H_4	O_3	μm (air)	NH_3	C_2H_4
$P(36)$	9.692			6.7	10.761		
$P(34)$	9.673		2.18	3.0	10.738	12.4	0.54
$P(32)$	9.655	0.31	0.72	5.9	10.716	15.0	0.48
$P(30)$	9.637	0.082	1.27	6.4	10.693	0.86	1.63
$P(28)$	9.619	0.056	0.24	9.4	10.672	0.36	1.30
$P(26)$	9.601	0.10	0.23	6.0	10.650	0.34	2.40
$P(24)$	9.584	0.43	0.42	0.7	10.629	0.13	2.10
$P(22)$	9.567	0.35	0.82	1.8	10.608	0.045	1.09
$P(20)$	9.550	2.16	0.40	5.5	10.588	0.12	1.64
$P(18)$	9.533	0.24	0.79	6.4	10.568	0.14	3.28
$P(16)$	9.517	0.20	0.20	9.0	10.549	0.49	4.55
$P(14)$	9.501	0.31	0.14	12.7	10.529	0.81	29.10
$P(12)$	9.486	0.94	0.16	12.2	10.510	0.57	4.35
$P(10)$	9.470	0.36	0.42	6.0	10.492	0.13	3.10
$P(8)$	9.455			12.7	10.473		
$R(8)$	9.340				10.331	21.9	0.99
$R(10)$	9.327	0.24	0.33		10.316	0.78	1.51
$R(12)$	9.315	0.34	0.082		10.301	0.46	1.94
$R(14)$	9.303	0.66	0.073		10.286	0.63	1.27
$R(16)$	9.291	12.7	0.28		10.272	0.10	1.04
$R(18)$	9.280	0.13	0.61		10.258	0.23	0.55
$R(20)$	9.269	0.027	0.17		10.244	0.036	1.27
$R(22)$	9.258	0.064	0.10		10.230	0.057	2.64
$R(24)$	9.247	0.064	0.18		10.217	0.038	5.04
$R(26)$	9.207	0.11	0.11		10.204	0.044	2.16
$R(28)$	9.227	0.38	0.046		10.192	0.044	2.35
$R(30)$	9.217		0.22		10.180	0.029	0.56
$R(32)$	9.208				10.168	0.020	0.83

*Reference 2

Table II. Relative transmission over 2 km range of CO_2 laser lines considered for remote sensing of NH_3, C_2H_4, CH_3OH and O_3.

Frequency $(cm)^{-1}$	CO_2 Laser Line I.D.	Relative Transmission I/I_o Midlatitude	
		Winter	Summer
931.002	*P(34)	.843	.344
932.961	*P(32)	.832	.338
934.895	*P(30)	.818	.328
947.743	*P(16)	.728	.264
949.480	*P(14)	.746	.297
951.193	*P(12)	.755	.310
1035.474	†P(32)	.807	.384
1037.434	†P(30)	.783	.399
1041.279	†P(26)	.738	.355
1043.163	†P(24)	.750	.356

* - (00°1)-(10°0) band
† - (00°1)-(02°0) band

Table III. CO_2 Laser lines for remote sensing by differential absorption.

Gas	CO_2 Laser Lines	
	On-Coincidence	Off-Coincidence
Ethylene	P(14) (00°1)-(10°0)	P(16) (00°1)-(10°0)
Ammonia	P(32) (00°1)-(10°0)	P(30) (00°1)-(10°0)
Ozone	P(26) (00°1)-(02°0)	P(24) (00°1)-(02°0)
Methanol	P(32) (00°1)-(02°0)	P(30) (00°1)-(02°0)

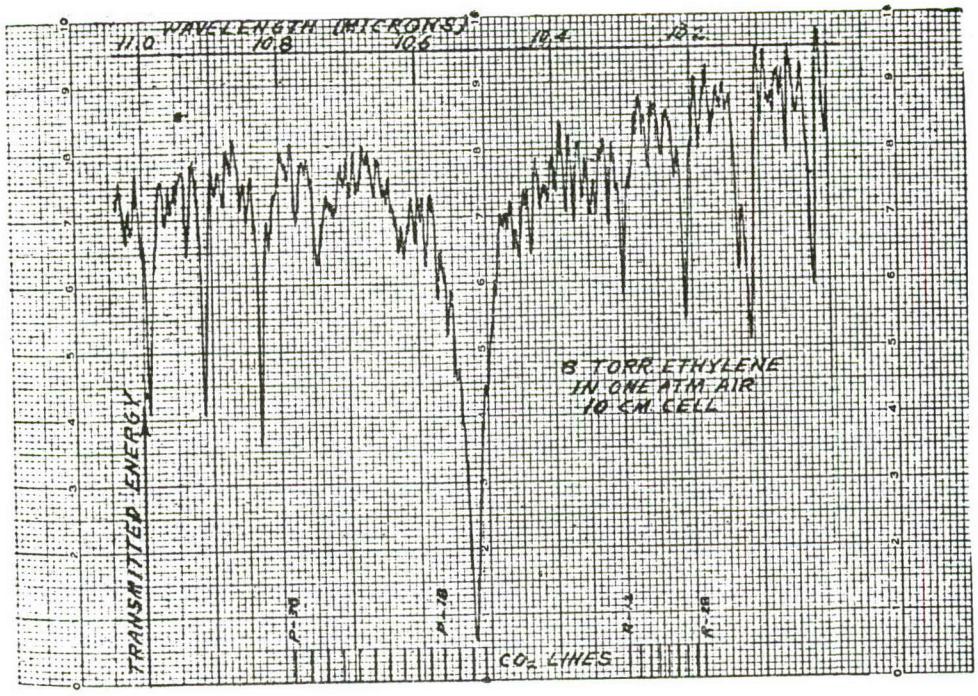

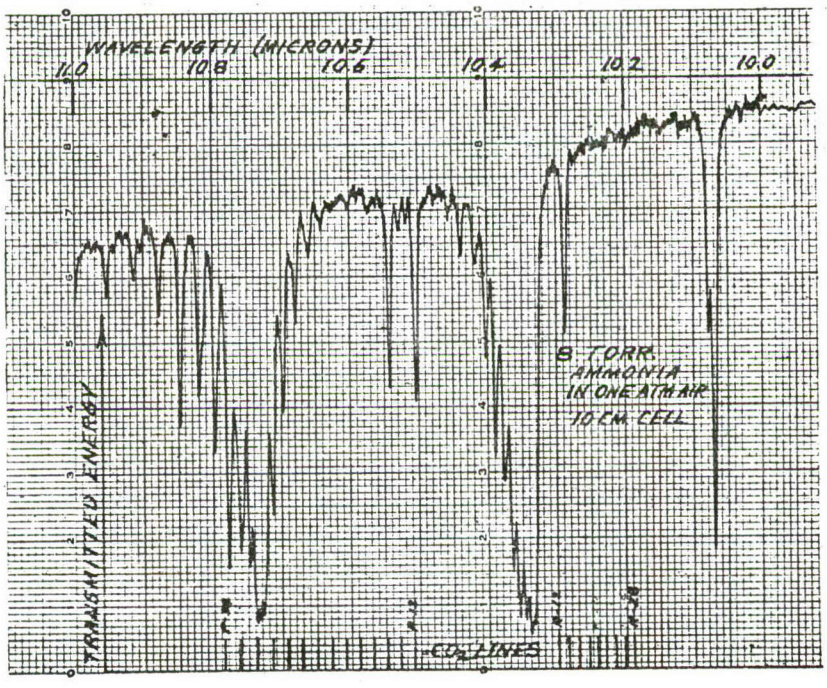

From Reference 1

Fig. 1

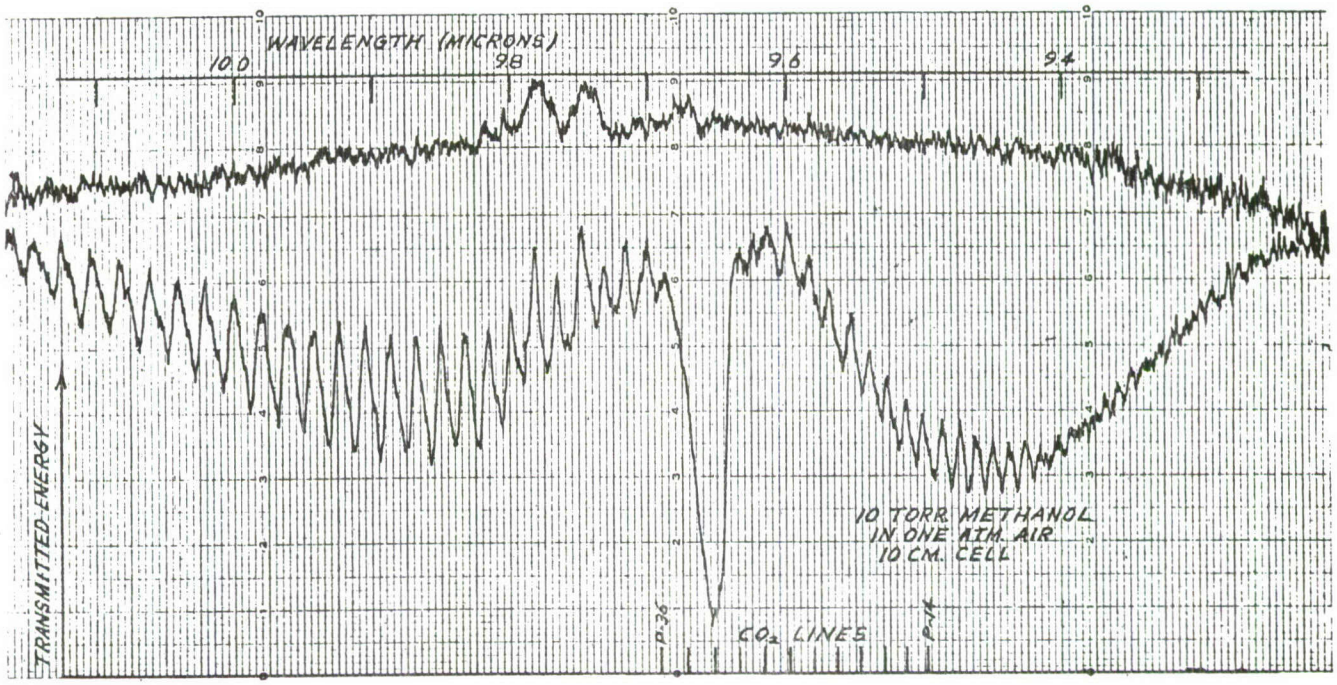

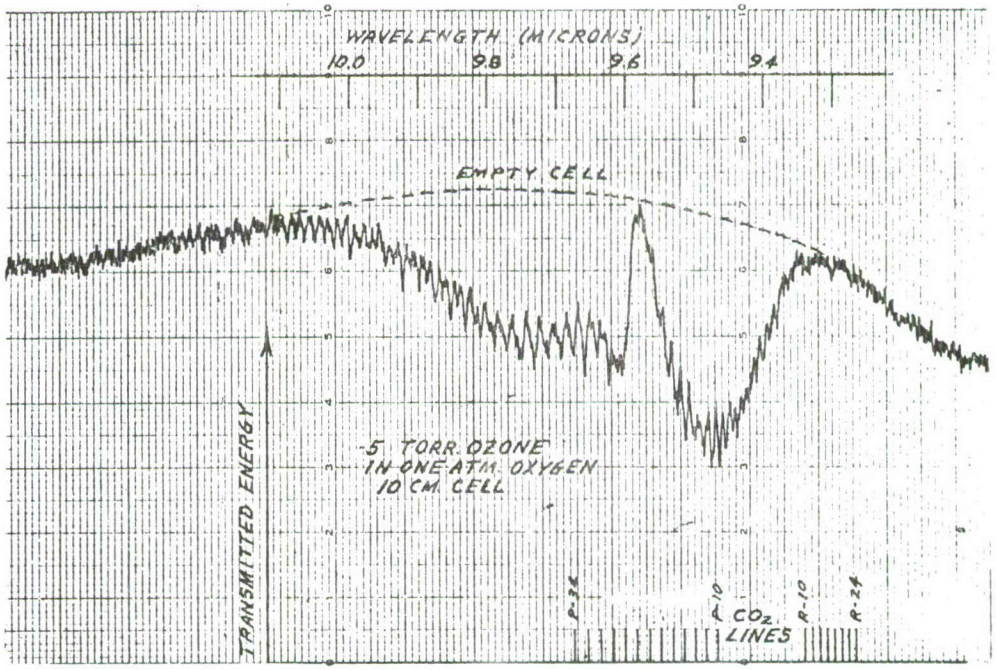

From Reference 1

Fig. 2

Appendix D

The following is a reprint of an internal Lincoln Laboratory memorandum titled "Range and Sensitivity Considerations of a Frequency-Doubled Mini-TEA CO_2 Laser for Remote Sensing of CO and NO".

MASSACHUSETTS INSTITUTE OF TECHNOLOGY
LINCOLN LABORATORY

7 February 1979

TO: A. Mooradian and P. L. Kelley

FROM: N. Menyuk

SUBJECT: Range and Sensitivity Considerations of a Frequency-Doubled Mini-TEA CO_2 Laser for Remote Sensing of CO and NO

In this memo I consider the energy requirements as a function of range for remote sensing of CO and NO for a system which uses the frequency-doubled output of a mini-TEA laser as the primary source of coherent radiation. The sensitivity of the system to the presence of these molecules is also considered. The calculations assume topographic backscatter from a diffuse reflector located a distance R from the transmitter and receiver, and the use of a differential absorption lidar (DIAL) technique in which the reflected response at the molecular absorption frequency is compared with reflection at a nearby nonabsorbing frequency.

In a previous memo, a study was made of all the frequencies where coincidences occurred between absorption lines of the 1-0 bands of CO and NO and the second harmonic of CO_2 laser lines. At ground level, with pressure broadening, coincidence was defined as a frequency difference $\Delta\nu < 0.1\ cm^{-1}$. It was found that the most suitable of these coincidences for remote sensing purposes, on the basis of atmospheric transmittance, absorption line intensity of the NO or CO molecule and power output of the mini-TEA laser were: 1) the doubled P(24) CO_2 laser line of the $(10^0 0)$-$(00^0 1)$ band with the $R(1/2)_{1/2}$ absorption line of NO and 2) the doubled P(24) CO_2 laser line of the $(10^0 0)$-$(02^0 0)$ band with the P(14) absorption line of CO. Table I gives the frequency values for the coincident lines and for the preferred neighboring non-resonant doubled-frequency line.

Table I also contains the values of the volume extinction coefficient $\beta_m(\lambda)$ at each of these wavelengths for two standard atmospheres, namely midlatitude summer and midlatitude winter.[1] The two-way transmittance T over a range R at

wavelength λ is defined by $T(\lambda) = \exp[-2\beta_m(\lambda) R]$.

The power received at the detector at a wavelength λ_2 which is off-resonance is given by

$$P_r(\lambda_2) = P_r^{off} = \frac{K(\lambda_2)\rho(\lambda_2) A P_o(\lambda_2) T(\lambda_2)}{\pi R^2} \tag{1}$$

where K is the receiver efficiency, ρ the reflectivity of the topographic reflector and P_o the output power at λ_2, and A is the area of the receiving telescope. At λ_1, which is on or near resonance,

$$P_r(\lambda_1) = P_r^{on} = \frac{K(\lambda_1)\rho(\lambda_1)A P_o(\lambda_1)T(\lambda_1)}{\pi R^2} \exp[-2n\sigma_m(\lambda_1) L] \tag{2}$$

where n is the pollutant density which extends over a distance L and $\sigma_m(\lambda_1)$ is the molecular absorption coefficient at λ_1. The value of σ_m is a function of the line intensity of the absorption line (S), the line width (α) and the frequency difference between the center of the absorption line (ν_o) and the radiation frequency (ν_1) according to the formula $\sigma_m = S\alpha/\pi[(\nu_1-\nu_o)^2 + \alpha^2]$.

For λ_1 and λ_2 representing neighboring CO_2 laser lines, it is reasonable to assume $K(\lambda_1) = K(\lambda_2) = K$ and $\rho(\lambda_1) = \rho(\lambda_2) = \rho$. Then, in the presence of the pollutant,

$$P_r^{off} - P_r^{on} = \frac{K\rho A}{\pi R^2} P_o(\lambda_2)T(\lambda_2)\left[1 - \frac{P_o(\lambda_1)T(\lambda_1)}{P_o(\lambda_2)T(\lambda_2)} \exp[-2n\sigma_m(\lambda_1)L]\right] \tag{3a}$$

while, in the absence of the pollutant, n = 0 and

$$P_r^{off} - P_r^{on})_{n=0} = \frac{K\rho A}{\pi R^2} P_o(\lambda_2)T(\lambda_2)\left[1 - \frac{P_o(\lambda_1)T(\lambda_1)}{P_o(\lambda_2)T(\lambda_2)}\right] . \tag{3b}$$

The difference, δ, between Eqs. (3a) and (3b) is the signal due to the presence of pollutant

$$\delta = \frac{K\rho A}{\pi R^2} P_o(\lambda_1) T(\lambda_1) \{1 - \exp[-2n\sigma_m(\lambda_1) L]\} \quad . \tag{4}$$

The minimum detectable value of δ occurs for S/N = 1, i.e., for $\delta = P_N = (NEP)(2\Delta f)^{1/2}$, which is the dark-current limited noise. The minimum energy per pulse is then given by

$$E_o^{min}(\lambda_1) = P_o^{min}(\lambda_1)\,\tau = \frac{2\pi R^2}{K\rho A} \times \frac{(NEP)\sqrt{\tau}}{T(\lambda_1)\{1 - \exp[-2n\sigma_m(\lambda_1) L]\}} \tag{5}$$

where we have taken the time-bandwidth product $\tau\Delta f = 2$. When results are averaged over a train of N pulses, the minimum energy requirement is reduced by the factor $1/\sqrt{N}$.

To this point the results are quite general. In applying Eq. (5) to the remote sensing of CO and NO, there is one major distinction. The NO is not normally present in the atmosphere; CO is. The presence of CO is included in the evaluation of the transmittance $T(\lambda_1)$, but on the basis of the standard atmospheres which assume a CO molecular density of 75 ppb. In many instances, the ambient atmosphere will contain many times this amount, in which case $T(\lambda_1)$ must be corrected. This situation will be discussed in greater detail below.

To evaluate Eq. (5), we assume an NEP = 3×10^{-12} W $Hz^{-1/2}$, $\rho = 0.5$ and $K = 0.1$.[2] Our effective telescope area $A \simeq 600$ cm^2 and $\tau \simeq 10^{-7}$ sec. Then

$$E_o(\lambda_1) \geq \frac{2 \times 10^{-6} R^2}{T(\lambda)\sqrt{N}\{1 - \exp[-2n\sigma_m(\lambda_1) L]\}} \tag{6}$$

where R is the range in km.

The value of σ_m at the chosen frequencies are 9.08×10^{-19} cm^2 for CO and 4.85×10^{-20} cm^2 for NO. Figure 1 evaluates the minimum energy per pulse vs range assuming a CO concentration of 100 ppm over a distance L = 50 m (for this high a product of nL, $e^{-2n\sigma_m(\lambda_1)L} \simeq 0$ for CO). A similar concentration of NO leads to the minimum energy per pulse vs range curves shown in Fig. 2. The higher energy required for a given range in NO as compared with CO is primarily due to the effect of water vapor absorption lines in the vicinity of the NO absorption. This accounts for the strong increase in required energy for the midlatitude summer atmosphere, where the water vapor density is a factor of 4 greater than in the midlatitude winter atmosphere. An additional significant factor is the lower value of σ_m for NO.

As was noted above, CO is normally present in the atmosphere. In the standard atmospheres used by McClatchey et al.[1], and which formed the basis for our values of σ_m (and hence $T(\lambda)$), the concentration of CO is taken to be 75 ppb. However, there is a great deal of variation in the amounts of CO listed as typical atmospheric concentrations, varying from the 0.075 ppm used here to a 0.1 ppm global average,[3] and from 0.3-1.0 ppm for rural environments to 15 ppm being considered typical for urban environments.[4] Additional CO in the ambient atmosphere can significantly increase the energy required for a given range by changing $T(\lambda)$ to $T'(\lambda)$ according to the relationship

$$T'(\lambda) = T(\lambda) e^{-2(\Delta n)\sigma_m(\lambda_1)R}$$

where Δn is the volume density of the ambient CO in excess of the 75 ppb included in $T(\lambda)$. The factor $T(\lambda)/T'(\lambda)$, which represents the increase in the minimum value $E_o^{min}(\lambda)$, is shown as a function of Δn for several ranges in Fig. 3. The effect of additional CO in the atmosphere is almost

catastrophic at the longer ranges, and may well be the primary limiting factor for the 2-3 km range in which we will be interested initially. It is clear from these results that an accurate determination of the ambient CO content over the range investigated will be essential.

The strong effect of ambient CO is due in part to the fact that the doubled CO_2 laser frequency and the P(14) absorption line are coincident to within .004 cm^{-1}. The R(2) absorption line of CO is also in very close coincidence with a doubled R(18) CO_2 laser frequency ($\Delta\nu \simeq 0.009\ cm^{-1}$) and has a slightly larger absorption cross-section; hence the use of the R(18) line would be subject to the same extinction effect. The other doubled CO_2 lines coincident with CO absorption have not been obtained with the mini-TEA laser (i.e., the doubled R(30) and R(8) of the 9.4 μm band). The effect shown in Fig. 3 will be somewhat mitigated by the line width of the coherent radiation. Since the CO_2 laser is at atmospheric pressure, a linewidth $\geq$ 1 GHz can reasonably be expected, resulting in a linewidth $\geq$ 2 GHz at the doubled frequency. This reduces the effective coincidence and, concomitantly, the effective value of σ_m. A reduced value of σ_m is not an unmixed blessing, however, since it adversely effects the section in brackets in the denominator of Eq. (6) and increases the minimum observable quantity of pollutant. In any event it will be necessary to determine the extent to which the value of σ_m for CO is affected by using the frequency doubled mini-TEA laser as the coherent radiation source. An experimental arrangement to do this will be set up shortly.

Using the mini-TEA laser with a mirror, a second harmonic output of over 2 mJ/pulse at a pulse repetition frequency of 400 Hz has been obtained. It is reasonable to anticipate that comparable values ($\sim$ 1 mJ/pulse) will be available from the P(24) lines in a grating system. For standard atmospheres, Fig. 1 indicates that, for the conditions considered, a 1 mJ pulse is sufficient to yield a 5-7 km range for remote sensing of CO with S/N = 1. For a one-second average over 400 pulses, a twenty-

fold increase in S/N is available or, alternatively, an increase in range to > 8.5 km. The ranges available for NO sensing are much lower. Under conditions of high water vapor presence in the atmosphere, as indicated by the midlatitude summer curve of Fig. 2, a range above 2 km is marginal. For the midlatitude winter atmosphere, on the other hand, a range of over 4 km is available for a single pulse of 1 mJ energy, rising to over 7 km on averaging over 400 pulses.

Finally, I'll now consider the minimum detectable pollution concentration, given our set up. From Eqs. (1) and (2),

$$2n\sigma_m(\lambda_1)L = \ell n\left[\frac{P_r(\lambda_2)P_o(\lambda_1)T(\lambda_1)}{P_r(\lambda_1)P_o(\lambda_2)T(\lambda_2)}\right] \quad . \tag{7}$$

Taking $P_o(\lambda_1) \simeq P_o(\lambda_2)$, which is a reasonable assumption for adjoining doubled CO_2 laser lines, and also substituting for $T(\lambda_1)$ and $T(\lambda_2)$

$$2n\sigma_m(\lambda_1)L = \ell n\left[\frac{P_r(\lambda_2)\, e^{2[\beta_m(\lambda_2)-\beta_m(\lambda_1)]R'}}{P_r(\lambda_1)}\right] \tag{8}$$

where R' is the range in km ($R' = R \times 10^{-5}$).

For $n = n_{min}$, the minimum detectable concentration of pollutant, we are generally in a regime where $2n\sigma_m(\lambda_1)L \ll 1$, so

$$n_{min} \simeq \frac{1}{2\sigma_m(\lambda_1)L}\left\{\frac{P_r(\lambda_2)e^{2[\beta_m(\lambda_1)-\beta_m(\lambda_2)]R'} - P_r(\lambda_1)}{P_r(\lambda_1)}\right\} \quad . \tag{9}$$

Most evaluations in the literature assume $\beta_m(\lambda_2) = \beta_m(\lambda_1)$. However, on the basis of transmittance evaluations at the various frequencies of interest, we know $\beta_m(\lambda_1) \neq \beta_m(\lambda_2)$ for remote sensing of either CO or NO using frequency doubled CO_2 laser radiation. The differences are fairly large and have different signs for the two molecules. There are two approaches generally taken to evaluate n_{min}. The

first is to determine the ultimate limitation by setting the difference in the return signals equal to the noise signal ($\Delta P_r = P_N$). The second, and more conservative approach, assumes a limitation in the ability to distinguish changes in the return signal ratios below some value (i.e., $\{\Delta P_r/P_r \geq .01\}$). We will consider both cases for both CO and NO.

For the case where $\Delta P_r = P_N$, with $P_r(\lambda_1)$ given in Eq. (1),

$$n_{min} = \frac{1}{2\sigma_m(\lambda_1)L} \left\{ \frac{\pi R^2 P_N \tau}{K\rho A E_o(\lambda_1) T(\lambda_1) \exp[-2n_{min}\sigma_m(\lambda_1)L]} \right\} . \quad (10)$$

Taking $\exp[-2n_{min}\sigma_m(\lambda_1)L] = 1$, $E_o(\lambda_1) = 1$ mJ and the values used previously for the other terms,

$$n_{min} = \frac{1}{2\sigma_m(\lambda_1)L} \left[\frac{2.0 R^2 \times 10^{-13}}{e^{-2\beta_m(\lambda_1) R'}} \right] . \quad (11)$$

When using topographic reflection for remote sensing, the amount of pollutant concentration determined is the average amount $\bar{n}$ over the entire range R, even though the pollution may be limited to a smaller region L. Thus $\bar{n}\, R = nL$ and

$$\bar{n}_{min} = \frac{R' \times 10^{-18}}{\sigma_m(\lambda_1)\, e^{-\beta_m(\lambda_1) R'}} \quad (12)$$

Evaluating Eq. (12) for CO leads to the results given in Fig. 4; a similar evaluation for NO is shown in Fig. 5. It is seen that the detector-limited sensitivity to CO is clearly adequate. For NO, the sensitivity becomes extremely poor under conditions of high humidity for a range above the order of a kilometer. This brings it to approximately the range limitation discussed above and in Fig. 2.

Equation (12) represents the ultimate in sensitivity for $\bar{n}_{min}$, and will not be achieved in practice. A more realistic approach is to assume the equipment will be

able to distinguish a change $\{\Delta P_r/P_r(\lambda_1)\} \geq 0.01$ in Eq. (9). In that case ,

$$n_{min} = \frac{5 \times 10^{-3}}{\sigma_m(\lambda_1) L} \quad \text{or} \quad \bar{n}_{min} = \frac{5 \times 10^{-3}}{\sigma_m(\lambda_1) R} \tag{13}$$

subject, of course, to detector noise limitations and range restrictions. The sensitivity limitation represented by Eq. (13) is shown as a dashed line in Figs. 4 and 5. The range limitation for a single 1 mJ pulse for the conditions assumed in Figs. 1 and 2 are also indicated in Figs. 4 and 5, respectively.

In conclusion, it is worthwhile considering our projected experiment of observing the NO and CO emission of a stationary aircraft located approximately 2 1/2 km from our remote sensing facility using topographic reflection in the light of the above results. Given standard atmospheres and the high CO emission content, neither range nor pollutant sensitivity should pose any problem. However, as Fig. 3 shows, a high ambient CO content will severely restrict the range. As for the emission, if it is sufficiently high, it may well eliminate any return at the absorbing frequency. If so, it will limit us to being able to set a minimum value on the product of the CO concentration and the region of the concentration.

As for NO, ones ability to operate over a 2 1/2 km range will depend strongly on the water vapor content of the atmosphere. For low humidity, as illustrated by the midlatitude winter atmosphere, there should be no serious problems in achieving the necessary sensitivity. With high water vapor content, such as in the midlatitude summer atmosphere, results will be marginal but we probably will be able to achieve the required results by averaging over a large number of pulses.

A study of the absorption of the frequency-doubled mini-TEA laser output by CO and NO of various concentrations at atmospheric pressure will be initiated for calibration purposes. It will also enable us to establish the extent to which the linewidth of the incident radiation reduces the drastic effect of high CO ambient concentration indicated in Fig. 3.

NM:az

REFERENCES

1. R. A. McClatchey, R. W. Fenn, J. E. A. Selby, F. E. Volz and J. S. Garing, Optical Properties of the Atmosphere (Third Edition), Environmental Research Paper, No. 411, AFCRL-72-0497 (1972).

2. R. L. Byer and M. Garbuny, Appl. Optics 12, 1496 (1973).

3. E. Robinson and R. C. Robbins, "Emissions, Concentrations and Fate of Gaseous Atmospheric Pollutants" in Air Pollution Control, Part II, W. Strauss, Editor, (Wiley-Interscience, 1972).

4. R. T. H. Collis and P. B. Russell, "Lidar Measurement of Particles and Gases by Elastic Backscattering and Differential Absorption" in Laser Monitoring of the Atmosphere, E. D. Hinkley, Editor, (Springer-Verlag, 1976).

APPENDIX D
FIGURE CAPTIONS

Fig. 1. Minimum energy per pulse as a function of range assuming a CO concentration of 100 ppm over a distance L = 50 m for standard midlatitude summer and winter atmospheres and topographic reflection.

Fig. 2. Minimum energy per pulse as a function of range assuming an NO concentration of 100 ppm over a distance L = 50 m for standard midlatitude summer and winter atmospheres and topographic reflection.

Fig. 3. Multiplicative factor by which minimum energy per pulse of Fig. 1 must be multipliedas a function of ambient CO content in excess of .075 ppm. The factor is given for several ranges.

Fig. 4. Minimum detectable average CO concentration by topographic reflection as a function of range using a single 1 mJ pulse. Solid lines represent ultimate detector-limited sensitivity for midlatitude summer and winter atmospheres. Dashed line represents sensitivity limitation as given by Eq. (13). Also shown are range limitations for a 1 mJ pulse, as given in Fig. 1 for midlatitude summer (R_{LS}) and winter (R_{LW}).

Fig. 5. Minimum detectable average NO concentration by topographic reflection as a function of range using a single 1 mJ pulse. Solid lines represent ultimate detector-limited sensitivity for midlatitude summer and winter atmospheres. Dashed line represents sensitivity limitation as given by Eq. (13). Also shown are range limitations for a 1 mJ pulse, as given in Fig. 2 for midlatitude summer (R_{LS}) and winter (R_{LW}).

Table I. Frequency-doubled lines for remote sensing.

CO_2 Laser Line	Absorption Line	$2\nu\ CO_2$- ABS	Volume Extinction Coefficient (β_m) Midlatitude Winter	Midlatitude Summer
P(24) (10°0)-(00°1) 2ν= 1881.0977	NO-R(1/2)1/2 ν=1881.0398	.0579 cm^{-1}	0.335 km^{-1}	1.445 km^{-1}
P(26) (10°0)-(00°1) 2ν=1877.3780			0.411 km^{-1}	1.694 km^{-1}
P(24) (10°0)-(02°0) 2ν=2086.3265	CO-(P14) ν=2086.3223	.0042 cm^{-1}	0.1654 km^{-1}	0.292 km^{-1}
P(26) (10°0)-(02°0) 2ν= 2082.5582			0.0334 km^{-1}	0.1077 km^{-1}

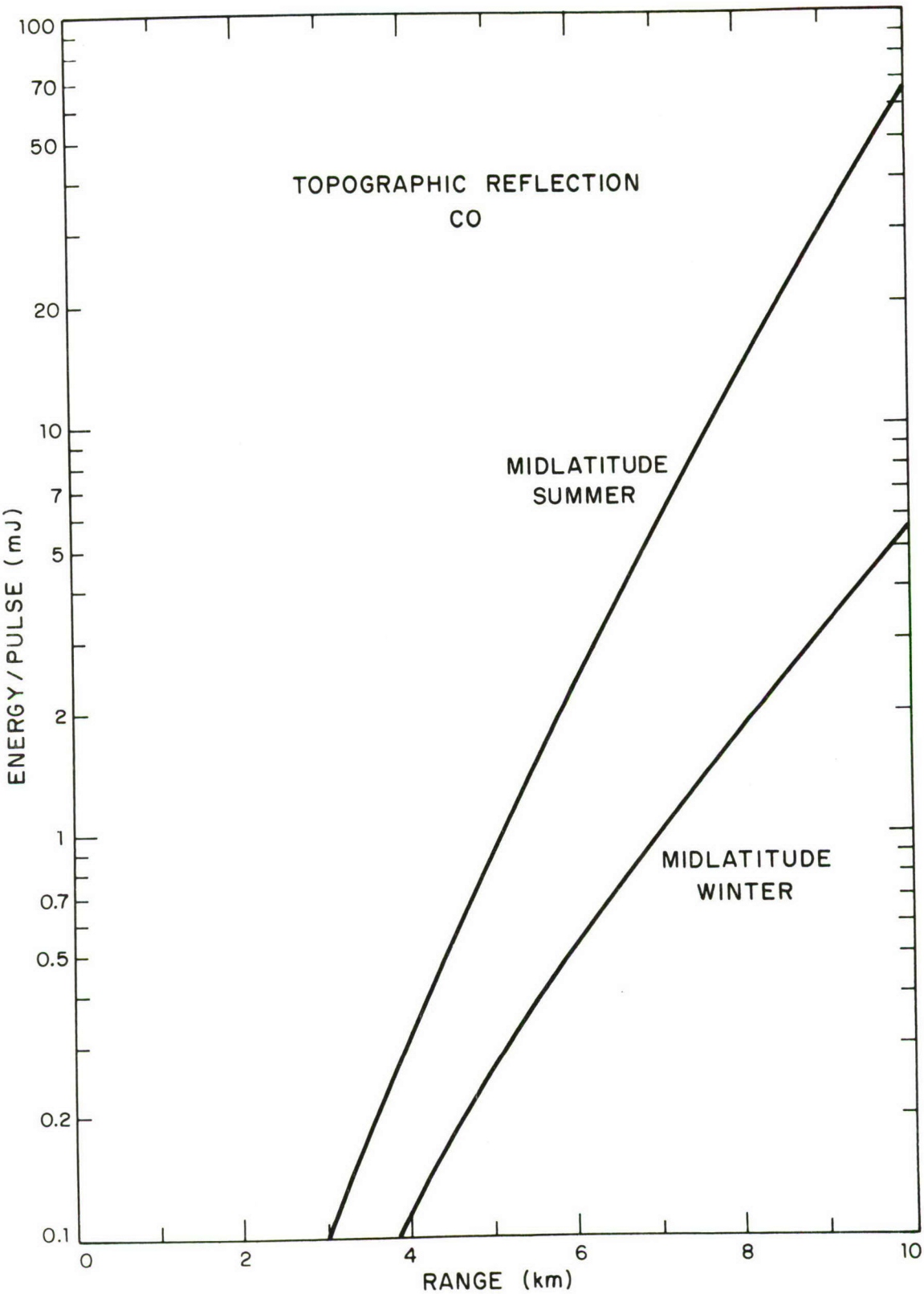
TOPOGRAPHIC REFLECTION
CO
MIDLATITUDE
SUMMER
MIDLATITUDE
WINTER
ENERGY / PULSE (mJ)
RANGE (km)
100
70
50
20
10
7
5
2
1
0.7
0.5
0.2
0.1
0
2
4
6
8
10

Fig. 1

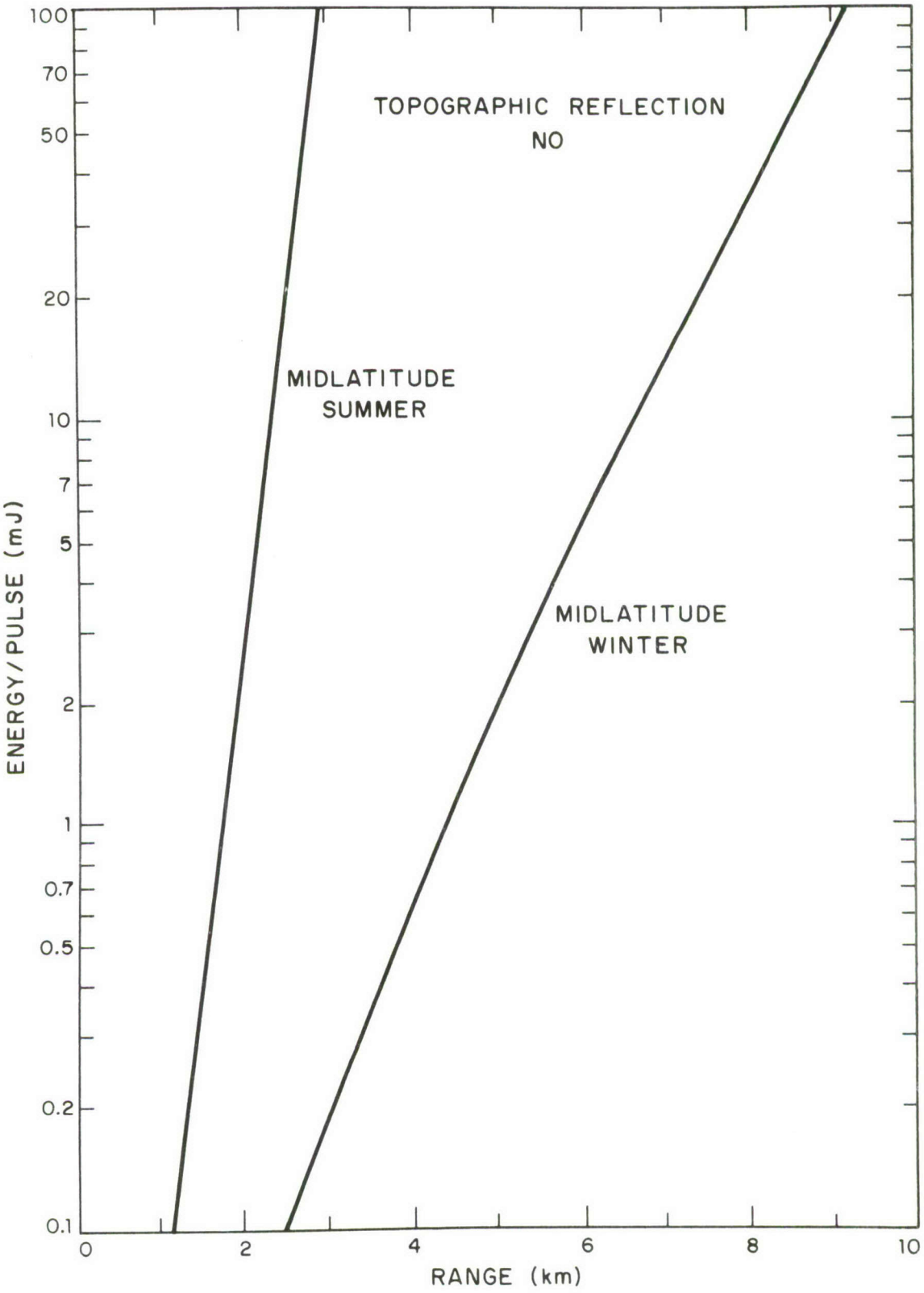
TOPOGRAPHIC REFLECTION
NO
MIDLATITUDE
SUMMER
MIDLATITUDE
WINTER
ENERGY/PULSE (mJ)
100
70
50
20
10
7
5
2
1
0.7
0.5
0.2
0.1
0
2
4
6
8
10
RANGE (km)

Fig. 2

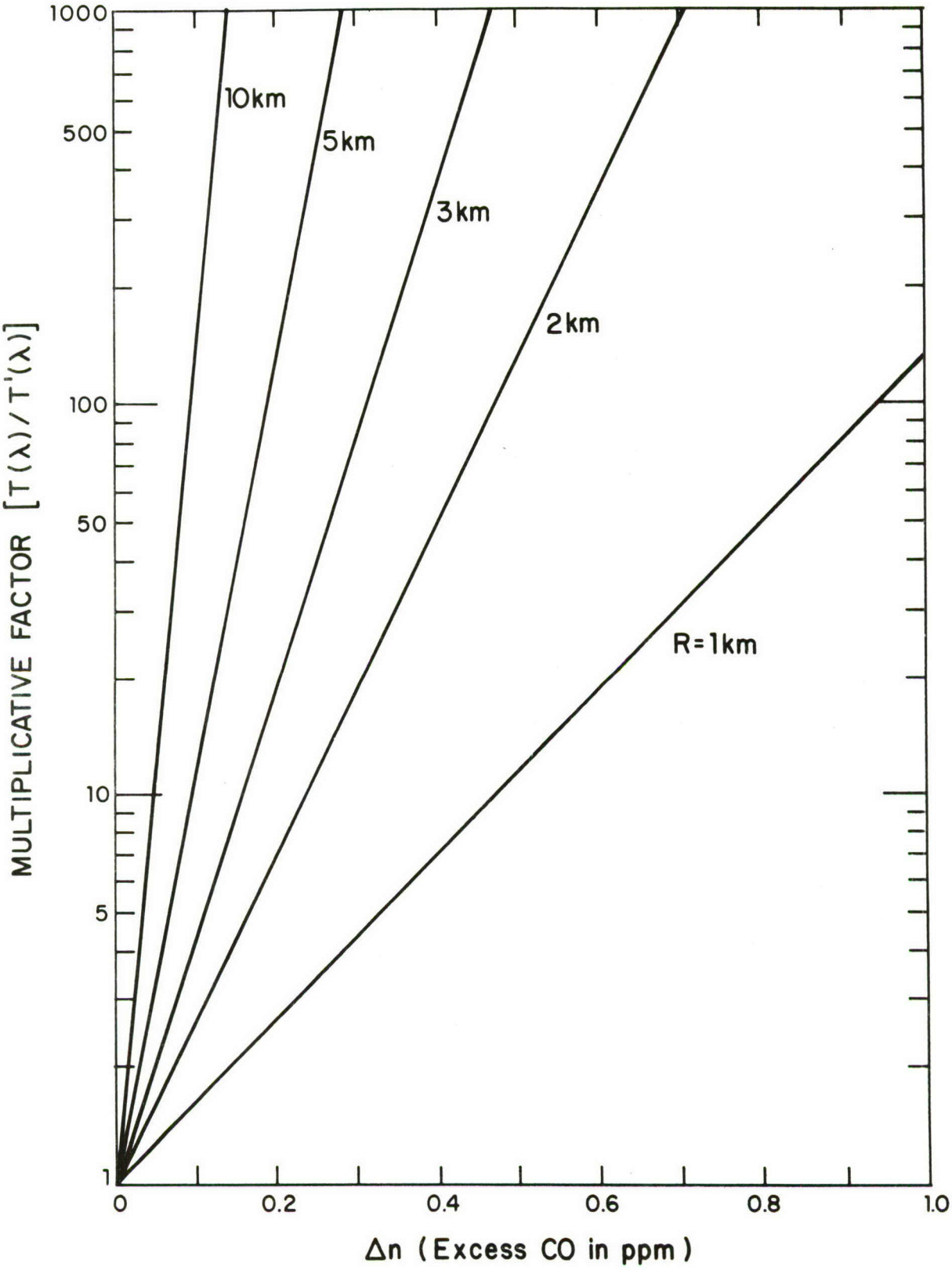
1000
500
100
50
10
5
1
10km
5km
3km
2km
R=1km
MULTIPLICATIVE FACTOR [T(λ)/T'(λ)]
0
0.2
0.4
0.6
0.8
1.0
Δn (Excess CO in ppm)

Fig. 3

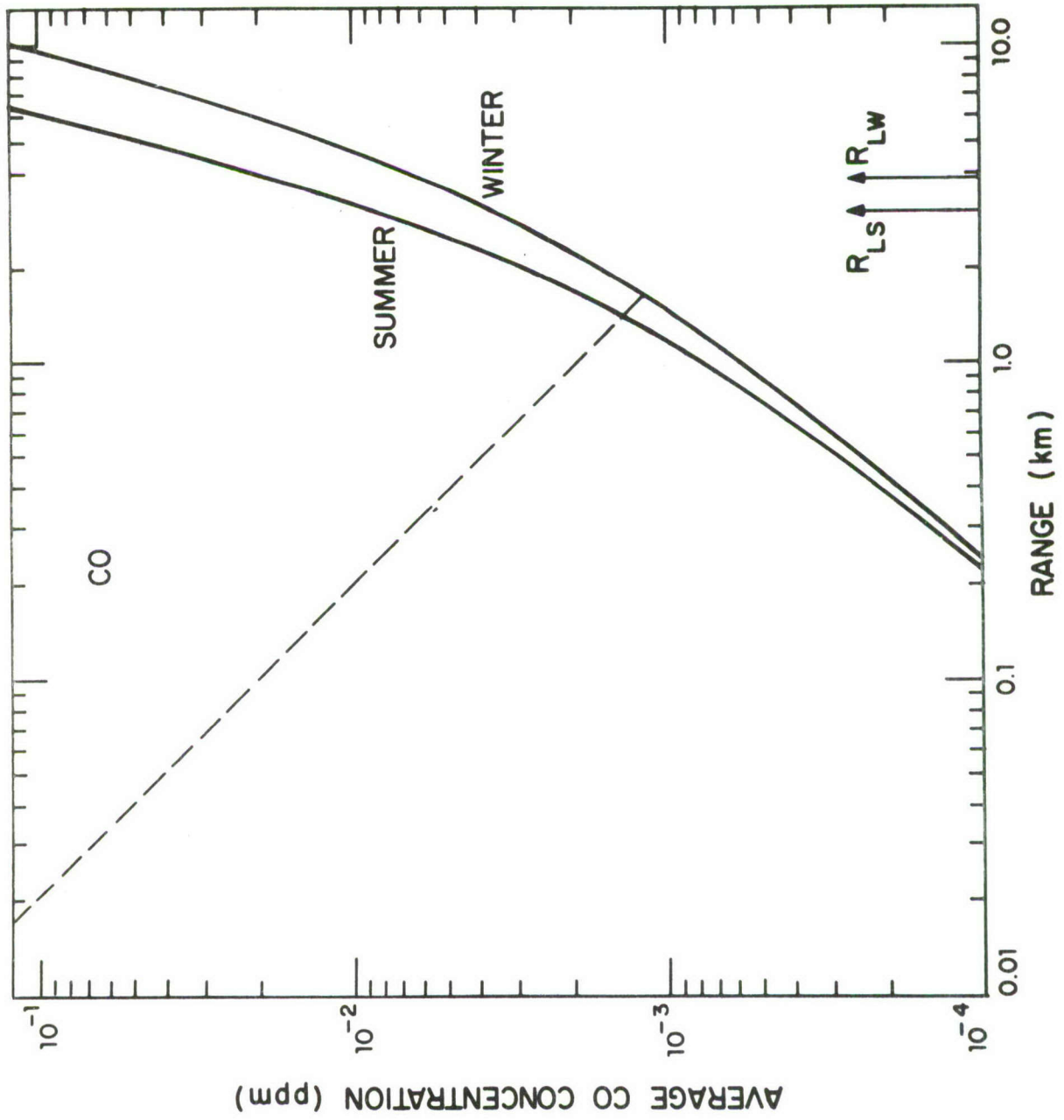
AVERAGE CO CONCENTRATION (ppm)
10^{-1}
10^{-2}
10^{-3}
10^{-4}
0.01
0.1
1.0
10.0
RANGE (km)
CO
SUMMER
WINTER
R_{LS}
R_{LW}

Fig. 4

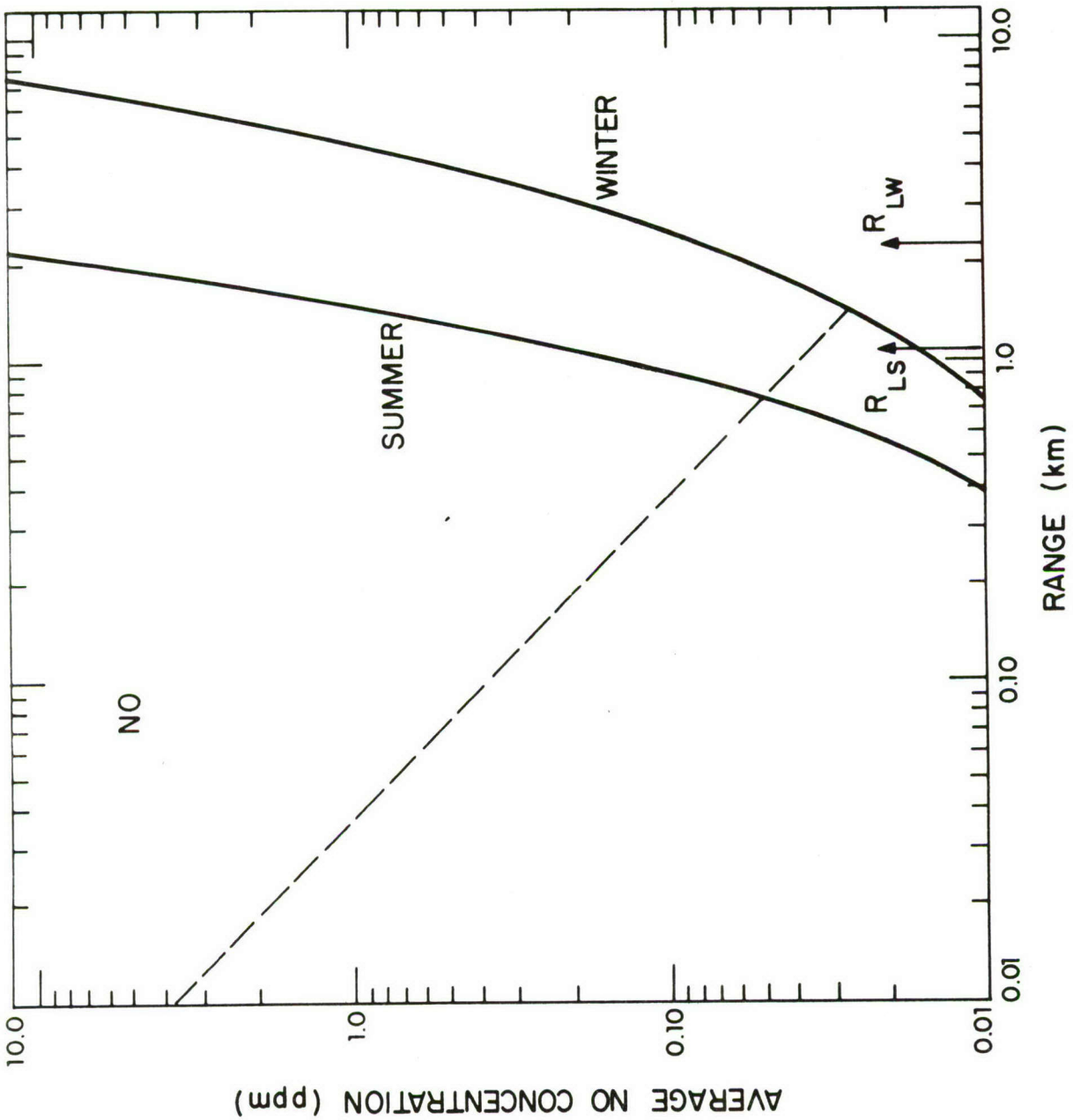
AVERAGE NO CONCENTRATION (ppm)
10.0
1.0
0.10
0.01
NO
SUMMER
WINTER
R_{LS}
R_{LW}
0.01
0.10
1.0
10.0
RANGE (km)

Fig. 5

Appendix E

The following is a preprint of a journal article to be published in Applied Physics Letters titled "Remote Sensing of CO Using Frequency-Doubled CO_2 Laser Radiation".

REMOTE SENSING OF CO USING FREQUENCY-DOUBLED CO_2 LASER RADIATION*

D. K. Killinger, N. Menyuk and W. E. DeFeo
Lincoln Laboratory, Massachusetts Institute of Technology
Lexington, Massachusetts 02173

Abstract

Single-ended remote sensing measurements of the atmospheric concentration of CO using differential-absorption of line-tunable, frequency-doubled CO_2 laser radiation near 4.6 μm are reported. The concentration of CO was deduced from laser backscatter returns from topographic targets at ranges up to 2.5 km with an overall uncertainty of approximately ± 10 ppb. The use of several targets at different ranges but along the same line-of-sight permitted pseudo-range resolved measurements and clearly established the strong localization of CO concentration over traffic roadways.

Preprint

(To be published in Applied Physics Letters.)

The measurement of trace constituents in the atmosphere has typically been conducted using conventional point-sampling techniques[1] such as gas chromotography, nondispersive IR spectrophotometry, and chemical reaction rate measurements. Recently, several laser remote sensing techniques utilizing laser-induced fluorescence,[2] Raman scattering,[3] and differential-absorption[4-7] of backscattered laser radiation have demonstrated significant advantages over these conventional methods. For the laser remote sensing of atmospheric constituents, studies[8,9] indicate that operation in the IR spectral region offers several advantages which include (1) the large number of molecules with distinct absorption transitions at these wavelengths, (2) the availability of relatively wide transmission windows in the atmosphere at the pertinent wavelengths, and (3) the relative degree of eye safety[10] provided by lasers operating in the IR as compared to the visible and UV region.

This letter reports the single-ended remote detection of CO in the atmosphere through the use of differential-absorption of line-tunable, frequency-doubled pulsed CO_2 laser radiation backscattered from topographic targets. Using this technique, we have measured the diurnal variation of the concentration of CO over a traffic roadway, the day-to-day variation of CO over a long path (2.5 km), and have observed the temporal variations in the atmospheric CO content due to momentary vehicular and aircraft traffic. Using several targets along the same line-of-sight, we have obtained the pseudo-range resolved measurement of atmospheric CO concentration and clearly established the strong localization of CO over traffic roadways. Our results may be compared to previous laser remote sensing measurements of atmospheric CO; these include measurements using low power tunable diode lasers near 4.7 μm with retroreflectors over path lengths up to 400 m[11,12] and single-ended topographic reflection measurements over a range of 107 m using parametric-oscillator radiation near 2.3 μm.[13] Our single-ended measurements represent a significant increase in sensitivity, detection range, and temporal resolution over these previous CO measurements.

A schematic of our experimental apparatus is shown in Fig. 1. A mini-TEA CO_2 laser[14] was used to generate line-tunable, pulsed radiation near 9.3 μm at repetition rates of up to 300 Hz. The frequency of the laser was tuned using a piezoelectric-controlled grating and monitored by a spectrometer to ensure stable single-line operation. The 9.3 μm radiation was frequency doubled in a $CdGeAs_2$ crystal.[15] The generated radiation near 4.65 μm had a pulse length of 70 ns and an energy per pulse ranging from 0.2 to 1 mJ. The spectral linewidth (FWHM) was measured and found to be approximately 0.02 cm^{-1}, which is considerably less than the pressure broadened linewidth of CO (0.14 cm^{-1}).[16]

Portions of the 4.65 μm output from the crystal were directed to a pyroelectric detector and also through a 50 cm absorption cell containing a calibrated mixture of 500 ppm of CO in air (ambient temperature and pressure). These signals provided a normalization of the laser intensity and a calibration of the CO absorption coefficient at the different laser transitions utilized. The remainder of the 4.65 μm radiation was sent through a x10 beam expander and directed by a 50 cm beam steering mirror toward topographic targets outside the laboratory. The angular divergence of the beam was measured to be approximately 0.4 mrad. Pulsed laser radiation backscattered from the target was collected by a collinear 30 cm Cassegrain telescope and detected with a 1 mm InSb detector located at the focal plane of the collection optics. The field of view of the telescope/detector was 1.11 mrad. The output signal from the InSb detector was processed through a gated boxcar integrator and normalized to the laser power through use of the reference pyroelectric detector output. Backscattered returns with a signal-to-noise ratio greater than 10 were easily observed from signs, telephone poles, trees, and foliage at ranges up to 1 km and from buildings at ranges up to 2.5 km.

For detection of CO using frequency-doubled radiation from our mini-TEA CO_2 laser, two absorption coincidences[17] may be utilized - the doubled R(18) line of CO_2 near 2154.604 cm^{-1} with the R(2) transition of CO near 2154.596 cm^{-1}, and the doubled P(24) line of CO_2 near 2086.326 cm^{-1} with the P(14) line of CO near 2086.322 cm^{-1}. The R(18) absorption coincidence is relatively free of interference from nearby absorption lines due to other atmospheric gases, while the P(24) line requires only slight correction due

to the presence of water vapor. This may be seen in Fig. 2 where the computer-generated synthetic transmission spectrum[18] of the atmosphere is shown along with the absorption coincidences and off-resonance lines of the doubled CO_2 laser radiation. It should be noted that the correction for the P(24) line due to water vapor is exaggerated in Fig. 2 due to the low resolution (0.25 cm^{-1}) of the shown synthetic transmission spectrum; the correction factor is less than 5% under the resolution conditions of our experiments.

The concentration of CO in the atmosphere, N_a, averaged over the path of the laser beam, is deduced from a comparison of the ratio of the on-resonance to the off-resonance laser backscatter with that obtained simultaneously from the laboratory absorption cell. This may be expressed approximately as

$$N_a = N_c \frac{\ell n (P_a/P_a')}{\ell n (P_c/P_c')} \frac{L}{2R} \left[1 + \frac{2R (\beta - \beta')}{\ell n (P_a/P_a')} \right] \tag{1}$$

where N_a is the deduced concentration of CO in the atmosphere, N_c is the CO concentration in the cell, L is the length of the cell, R is the one-way propagation range of the LIDAR beam, P_a is the normalized on-resonance laser backscattered signal strength, P_c is the normalized on-resonance absorption cell signal, and β is the frequency-dependent absorption coefficient[19] of the atmosphere not including the contribution from CO. The prime indicates off-resonance values and the subscripts a and c indicate atmospheric and absorption cell values, respectively. Equation (1) is valid for the case where $\beta_a = \beta_c \equiv \beta$ and $N_c >> N_a$ such that $|L(\beta-\beta')| << |\ell n (P_c/P_c')|$. These conditions were valid for our experiments. In addition, as seen in Fig. 2, the term containing $(\beta-\beta')$ in Eq. (1) is negligible for measurements obtained using the R(18) and R(20) transitions, and represents less than a 5% correction factor in the case of the P(24) and P(26) transitions.

Figure 3 shows the deduced atmospheric concentration of CO obtained over a 13 hour period[20] for a path which traversed a main traffic roadway located 480 m from the laboratory. The topographic target used was a painted

sign located approximately 20 m on the far side of the traffic roadway. These results were obtained using the R(18) absorption coincidence; results obtained using the P(24) coincidence (after correction for atmospheric water vapor)[19] were in agreement within our experimental uncertainty. For demonstration purposes, the diurnal variation of CO shown in Fig. 3 was obtained by smoothing the collected data over 15 minute intervals. The figure clearly reflects the increased vehicular traffic during the periods of morning arrival, lunch-time and evening departure of a working day. The actual time resolution was on the order of a few seconds. Under light traffic conditions, momentary large increases in the measured CO concentration were observed to be directly correlated to the passage of individual cars and trucks along the roadway.

Pseudo-range resolved measurements were obtained by utilizing several targets at different ranges along the same line-of-sight and differentiating the integrated path measurements obtained for the different ranges. As an example, Fig. 4 shows the pseudo-range resolved CO concentration measured for targets located at ranges of 200 m, 375 m, and 500 m along the same line-of-sight as that shown in Fig. 3. The two sets of data shown in Fig. 4 were taken at different times, one when the traffic on the roadway located at a range of 480 m was relatively heavy and the other when it was relatively light. Figure 4 clearly reflects the strong localization of CO due to emission from vehicular traffic.

Atmospheric CO measurements were also obtained from topographic targets at a range of 2.5 km. The results[21] indicated a long-term day-to-day stability, with the average CO concentration generally staying between 160 and 250 ppb with an overall uncertainty of ± 10 ppb. Short-term increases in the CO concentration on the order of 50-100 ppb were observed during the course of a day and were often correlated to aircraft or vehicular movement near the laser line-of-sight. For example, measurements obtained when a turbine powered helicopter flew into the line-of-sight at a range of 2.4 km indicated a localized CO concentration near the aircraft greater than 2.0 ppm if it is assumed that the increased CO concentration is confined to a region within 50 m of the aircraft.

The effect of atmospheric turbulence was investigated under the conditions of our experiments. Short-term fluctuations of the returned signals over the 5 km round-trip propagation path were approximately 5%. This is much smaller than the value of either the returned signals or $\ell n\,(P_a/P_a')$ and corresponds to an uncertainty on the order of ± 2 ppb/km, which is negligible compared to the measured CO concentration. We are currently implementing a digital data acquisition system, and preliminary results have indicated enhanced detection sensitivity of approximately an order of magnitude; under such conditions the corresponding effect of atmospheric turbulence would be significant compared to the system sensitivities and will require further study to better quantify its effect.

We would like to acknowledge the technical assistance of E. Casazza and the helpful discussions with P. L. Kelley and A. Mooradian. In particular, we wish to thank P. Moulton for his contribution to the design and development of the laser remote sensing system. This work was supported by the Department of the Air Force, in part with specific funding from the Air Force Engineering Services Center.

REFERENCES

1. J. H. Seinfeld, Air Pollution (McGraw-Hill, New York 1975).
2. C. C. Wang and L. I. Davis, Jr., Phys. Rev. Lett. 32, 349 (1974).
3. J. A. Cooney, Appl. Phys. Lett. 12, 40 (1968).
4. R. A. Baumgartner and R. L. Byer, Opt. Lett. 2, 163 (1978).
5. K. Asai, T. Itabe and T. Igarashi, Appl. Phys. Lett. 35, 60 (1979).
6. E. R. Murray, R. D. Hake, Jr., J. E. van der Laan and J. G. Hawley, Appl. Phys. Lett. 28, 542 (1976).
7. K. W. Rothe, U. Brinkmann and H. Walther, Appl. Phys. 4, 181 (1974).
8. H. Kildal and R. L. Byer, Proc. IEEE 12, 1644 (1971).
9. R. L. Byer, Opt. and Quant. Elect. 7, 147 (1975).
10. American National Standard for the Safe Use of Lasers, ANSI Z136-1976.
11. R. T. Ku, E. D. Hinkley and J. O. Sample, Appl. Opt. 14, 854 (1975).
12. L. W. Chaney, D. G. Rickel, G. M. Russwurm and W. A. McClenny, Appl. Opt. 18, 3004 (1979).
13. T. Henningsen, M. Garbuny and R. L. Byer, Appl. Phys. Lett. 24, 242 (1974).
14. N. Menyuk and P. F. Moulton, Rev. Sci. Instr. (to be published).
15. N. Menyuk, G. W. Iseler and A. Mooradian, Appl. Phys. Lett. 29, 422 (1976).
16. R. H. Hunt, R. A. Toth and E. K. Plyler, J. Chem. Phys. 49, 1968 (1968).
17. H. Kildal, R. S. Eng and A. H. M. Ross, J. Mol. Spectr. 53, 479 (1974).
18. R. J. Nordstrom, J. H. Shaw, W. R. Skinner, J. G. Calvert, W. H. Chan and W. M. Uselman, Env. Sci. Res. Lab. Report No. EPA-600/3-77-026, 1977.
19. R. A. McClatchey and A. P. D'Agati, AFGL Technical Report 78-0029, 1978.
20. Meterological conditions were approximately: 60°F-75°F, 60-70% rel. humidity, clear day, light winds. Date: 6 July 1979.
21. Meterological conditions were approximately: 70°F-80°F, 60% rel. humidity, moderate winds. Dates: 14-16 August 1979.

FIGURE CAPTIONS

Fig. 1. Schematic of experimental apparatus for laser remote sensing measurements.

Fig. 2. Synthetic transmission spectrum (Ref. 18) of the atmosphere (3 km path length, 29% relative humidity) and spectral position of the doubled-CO_2 laser frequencies useful for CO detection.

Fig. 3. Measured diurnal variation of average atmospheric CO concentration over a 13 hour period for a path length of 500 m which traversed a major traffic roadway located at a distance of 480 m.

Fig. 4. Pseudo-range resolved measurements of atmospheric CO deduced from differentiation of integrated path measurements. The laser returns were obtained from targets located at 200 m, 375 m, and 500 m along the same line-of-sight. The path for the farthest target at 500 m encompassed the traffic roadway located at 480 km.

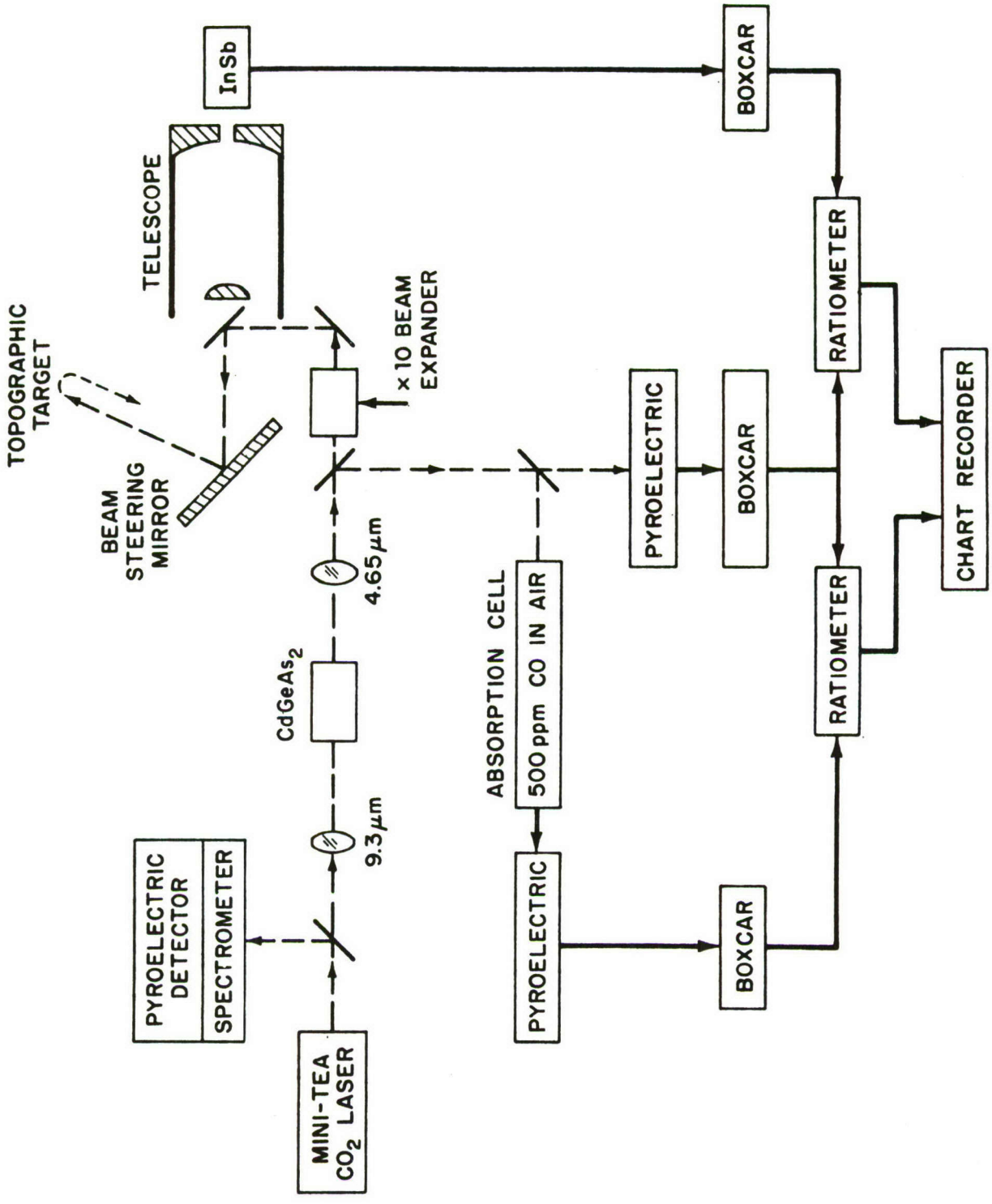
MINI-TEA
CO_2 LASER
PYROELECTRIC
DETECTOR
SPECTROMETER
9.3μm
$CdGeAs_2$
4.65μm
BEAM
STEERING
MIRROR
TOPOGRAPHIC
TARGET
TELESCOPE
× 10 BEAM
EXPANDER
ABSORPTION CELL
500 ppm CO IN AIR
PYROELECTRIC
PYROELECTRIC
InSb
BOXCAR
BOXCAR
BOXCAR
RATIOMETER
RATIOMETER
CHART RECORDER

Fig. 1

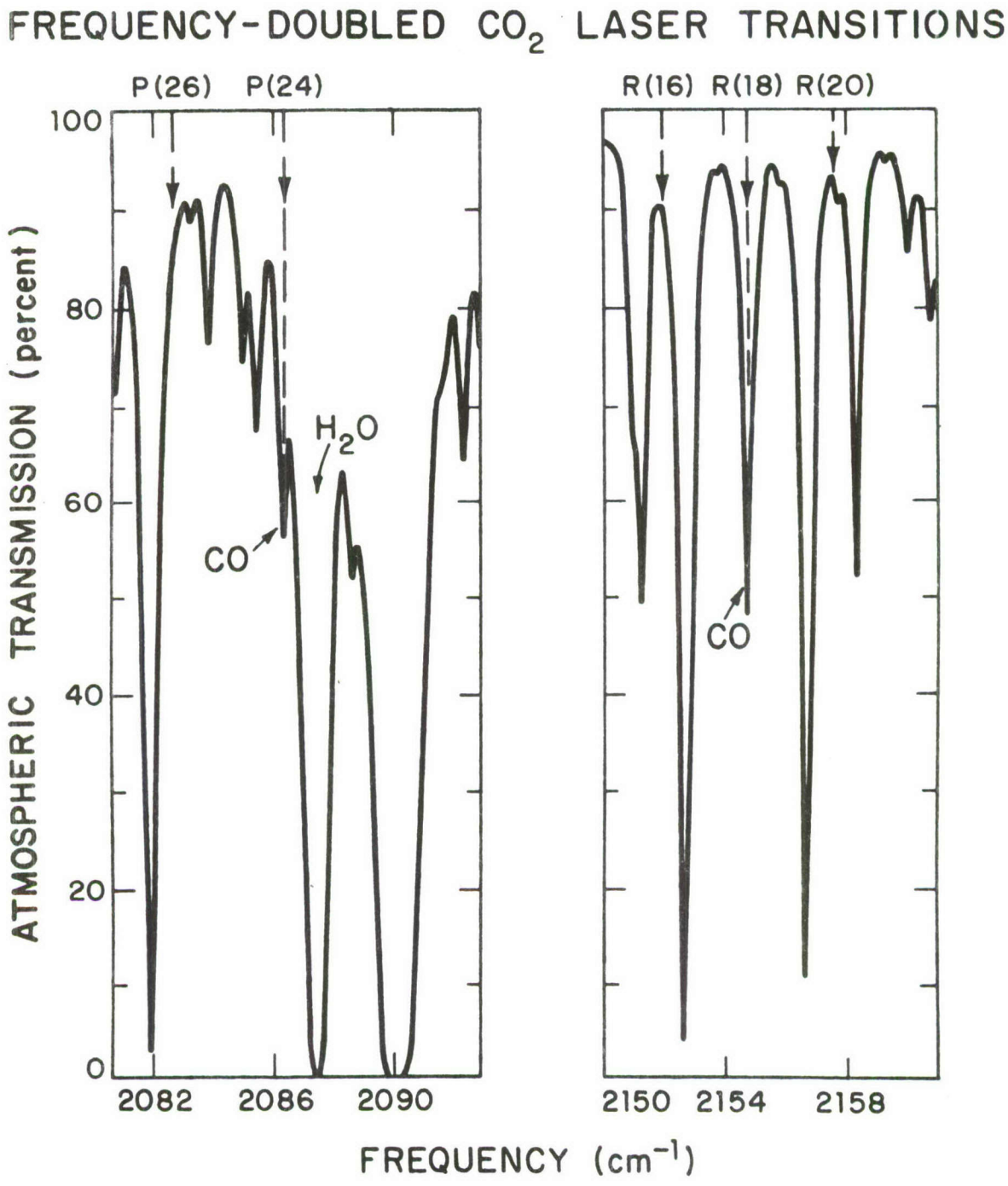
FREQUENCY-DOUBLED CO_2 LASER TRANSITIONS
P(26) P(24)
R(16) R(18) R(20)
100
80
60
40
20
0
ATMOSPHERIC TRANSMISSION (percent)
H_2O
CO
CO
2082
2086
2090
2150
2154
2158
FREQUENCY (cm^{-1})

Fig. 2

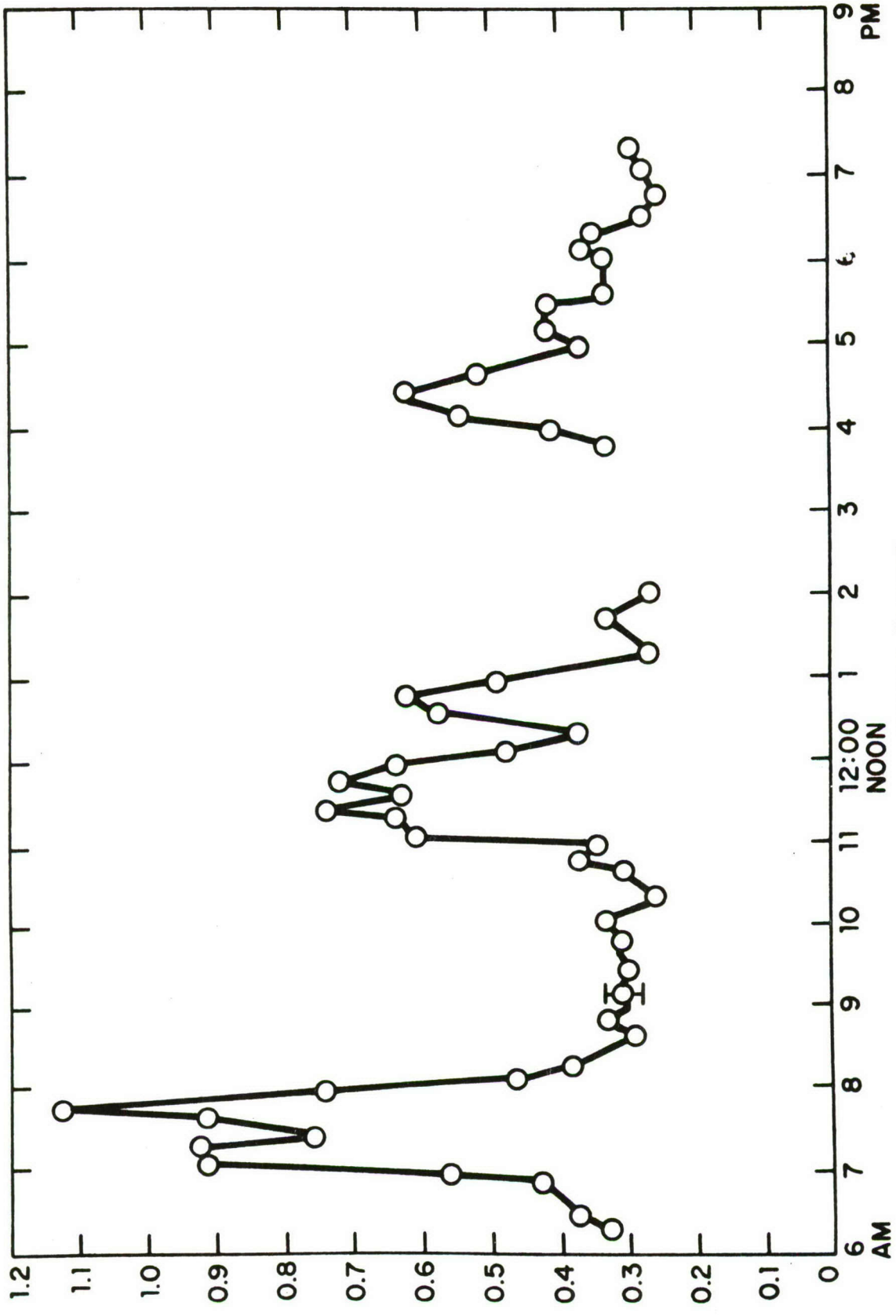
ATMOSPHERIC CO CONCENTRATION (ppm)
1.2
1.1
1.0
0.9
0.8
0.7
0.6
0.5
0.4
0.3
0.2
0.1
0
6 AM
7
8
9
10
11
12:00 NOON
1
2
3
4
5
6
7
8
9 PM
TIME (EDT)

Fig. 3

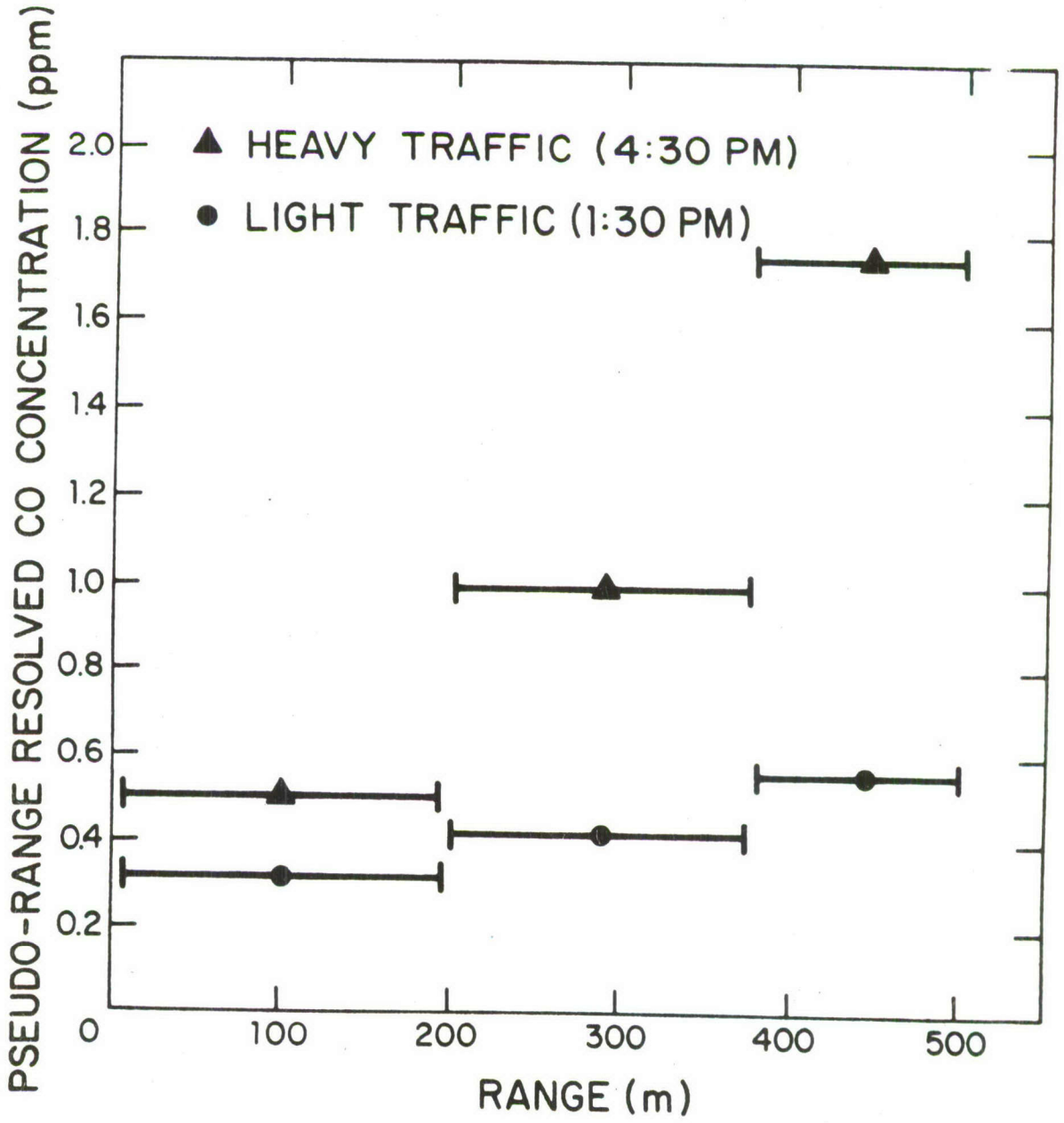
PSEUDO-RANGE RESOLVED CO CONCENTRATION (ppm)
2.0
1.8
1.6
1.4
1.2
1.0
0.8
0.6
0.4
0.2
0
HEAVY TRAFFIC (4:30 PM)
LIGHT TRAFFIC (1:30 PM)
100
200
300
400
500
RANGE (m)

REPORT DOCUMENTATION PAGE

READ INSTRUCTIONS BEFORE COMPLETING FORM

1. REPORT NUMBER ESD-TR-79-319 ESL-TR-80-09	2. GOVT ACCESSION NO.
3. RECIPIENT'S CATALOG NUMBER	
4. TITLE *(and Subtitle)* Remote Sensing of Turbine Engine Gases	5. TYPE OF REPORT & PERIOD COVERED Final Report 15 July 1978 – 30 September 1979
	6. PERFORMING ORG. REPORT NUMBER
7. AUTHOR*(s)* Aram Mooradian, Dennis K. Killinger, Norman Menyuk	8. CONTRACT OR GRANT NUMBER*(s)* F19628-78-C-0002
9. PERFORMING ORGANIZATION NAME AND ADDRESS Lincoln Laboratory, M.I.T. P.O. Box 73 Lexington, MA 02173	10. PROGRAM ELEMENT, PROJECT, TASK AREA & WORK UNIT NUMBERS Program Element No. 62601F Project No. 1900
11. CONTROLLING OFFICE NAME AND ADDRESS Engineering and Services Laboratory Air Force Engineering and Services Center Tyndall AFB, FL 32403	12. REPORT DATE 30 September 1979
	13. NUMBER OF PAGES 84
14. MONITORING AGENCY NAME & ADDRESS *(if different from Controlling Office)* Electronic Systems Division Hanscom AFB Bedford, MA 01731	15. SECURITY CLASS. *(of this report)* Unclassified
	15a. DECLASSIFICATION DOWNGRADING SCHEDULE

16. DISTRIBUTION STATEMENT *(of this Report)*

Approved for public release; distribution unlimited.

17. DISTRIBUTION STATEMENT *(of the abstract entered in Block 20, if different from Report)*

18. SUPPLEMENTARY NOTES

None

19. KEY WORDS *(Continue on reverse side if necessary and identify by block number)*

laser remote sensing
turbine engine gases
environmental monitoring
tactical detection and discrimination
miniature CO_2 TEA laser
LIDAR (DIAL) system
differential-absorption measurements
remote detection of CO

20. ABSTRACT *(Continue on reverse side if necessary and identify by block number)*

This is the final report for a laser remote sensing research program conducted by Lincoln Laboratory. The research conducted was designed to develop and demonstrate laser remote sensing techniques for monitoring jet aircraft exhaust gases.

The specific tasks which were performed consisted of the following: (1) development of an improved repetition rate miniature CO_2 TEA laser and incorporation into a differential-absorption LIDAR (DIAL) system, (2) laboratory demonstration of the frequency-doubled CO_2 TEA laser system by differential-absorption measurements of known gas samples (CO and NO), and (3) initial field feasibility demonstration of laser remote detection of CO in vehicular exhaust (automobile, tractor mower, and Skycrane helicopter) at ranges up to 2.5 km.